Human-like hip joint loading in *Australopithecus africanus* and *Paranthropus robustus*

Timothy M. Ryan[a,b,*], Kristian J. Carlson[c,d], Adam D. Gordon[e], Nina Jablonski[a], Colin N. Shaw[f], Jay T. Stock[f,g]

[a] *Department of Anthropology, Pennsylvania State University, University Park, PA, USA*

[b] *Center for Quantitative Imaging, Energy and Environmental Sustainability Laboratories, Institutes for Energy and the Environment, Pennsylvania State University, University Park, PA, USA*

[c] *Department of Integrative Anatomical Sciences, Keck School of Medicine, University of Southern California, Los Angeles, CA, USA*

[d] *Evolutionary Studies Institute, University of the Witwatersrand, Johannesburg, South Africa*

[e] *Department of Anthropology, University at Albany - SUNY, Albany, NY, USA*

[f] *PAVE Research Group, Department of Archaeology, University of Cambridge, Cambridge, UK*

[g] *Department of Anthropology, Western University, London, Ontario, Canada, N6A 3K7*

* Corresponding author.

  E-mail address: tmr21@psu.edu (Timothy M. Ryan).

1 **Abstract**

2

3 Adaptations indicative of habitual bipedalism are present in the earliest recognized hominins.

4 However, debate persists about various aspects of bipedal locomotor behavior in fossil hominins,

5 including the nature of gait kinematics, locomotor variability across different species, and the

6 degree to which various australopith species engaged in arboreal behaviors. In this study, we

7 analyze variation in trabecular bone structure of the femoral head using a sample of modern

8 humans, extant non-human hominoids, baboons, and fossil hominins attributed to

9 *Australopithecus africanus*, *Paranthropus robustus*, and the genus *Homo*. We use µCT data to

10 characterize the fabric anisotropy, material orientation, and bone volume fraction of trabecular

11 bone to reconstruct hip joint loading conditions in these fossil hominins. Femoral head trabecular

12 bone fabric structure in australopiths is more similar to that of modern humans and Pleistocene

13 *Homo* than extant apes, indicating that these australopith individuals walked with human-like hip

14 kinematics, including a more limited range of habitual hip joint postures (e.g., a more extended

15 hip) during bipedalism. Our results also indicate that australopiths have robust femoral head

16 trabecular bone, suggesting overall increased loading of the musculoskeletal system comparable

17 to that imposed by extant apes. These results provide new evidence of human-like bipedal

18 locomotion in Pliocene hominins, even while other aspects of their musculoskeletal systems

19 retain ape-like characteristics.

20

21 **Key words:** Trabecular bone; Hominin evolution; Bipedalism; Anisotropy

22

23

1. Introduction

Pliocene hominins display a variety of adaptations for habitual terrestrial bipedalism (Stern, 2000; Ward, 2013), but some aspects of their gait kinematics, locomotor variability, and the amount and nature of arboreality in their behavioral repertoires (i.e., its selective importance) remain unresolved (Ward, 2002; Lovejoy et al., 2009; Harcourt-Smith, 2016). Recent fossil evidence suggests that there may have been considerable locomotor variability among early hominins, and among australopiths in particular (Lovejoy et al., 2009; Zipfel et al., 2011; Haile-Selassie et al., 2012; DeSilva et al., 2013; Harcourt-Smith, 2016). Reconstruction of australopith gait kinematics has typically relied on interpretations of a variety of morphological characteristics, biomechanical models, fossilized trackways, and experimental studies of locomotor energetics (Ruff, 1995, 2010; Stern, 2000; Wang et al., 2003, 2004; Lovejoy, 2005b, a, 2007; Nagano et al., 2005; Sellers et al., 2005; Sockol et al., 2007; Raichlen et al., 2008, 2010; Lovejoy and McCollum, 2010; Kibii et al., 2011; Ward et al., 2011; Barak et al., 2013; Hatala et al., 2016; Dowdeswell et al., 2017; Raichlen and Gordon, 2017). While many of these studies agree that australopiths likely walked with relatively extended lower limbs rather than with a bent-hip, bent-knee (BHBK) gait (e.g., similar to the bipedal kinematics of chimpanzees; Sockol et al., 2007; Crompton et al., 2008), debate continues as to whether other kinematic aspects of their gait may have differed from those of later hominins and modern humans (DeSilva et al., 2013; Harcourt-Smith, 2016; Hatala et al., 2016; Su and Carlson, 2017). Recent fossil discoveries and comparative analyses have also refocused attention on the degree to which australopiths engaged in selectively advantageous arboreal locomotor behaviors (DeSilva, 2009; Zipfel et al., 2011; Green and Alemseged, 2012; Haile-Selassie et al., 2012; Churchill et al., 2013; Kappelman et al., 2016; Ruff et al., 2016; Rein et al., 2017). Debate about locomotor kinematics and the degree of arboreality in australopiths and

47 other early hominins often centers on interpretation of the functional significance of apparently

48 primitive traits associated with arboreal locomotion in these fossil taxa (Ward, 2002). The retention

49 of primitive features associated with arboreality in australopiths suggests either that these traits

50 were not detrimental or that they may have provided some adaptive advantage (Ward, 2002),

51 although differentiating between these scenarios is difficult (Lauder, 1996).

52 Biomechanically informative phenotypically plastic traits, or ecophenotypic traits, have the

53 potential to provide significant insight into the mechanical environment and specific behaviors that

54 an animal engaged in throughout its life (Ruff et al., 1999, 2016; Barak et al., 2013; Ward, 2013).

55 Because of the mechanosensitivity of bone during development, structural variation in both

56 cortical and trabecular bone provides insight into limb use and joint loading in extant and extinct

57 organisms (Pearson and Lieberman, 2004; Ruff et al., 2006). Trabecular bone, in particular, not

58 only has the potential to reveal important information about the magnitude and frequency of

59 loading, but also can inform interpretations of the directionality of joint reaction forces and, by

60 extension, provide insight into joint posture and loading. The distribution of trabecular bone

61 material in three-dimensional space is highly correlated with its mechanical behavior (Mittra et al.,

62 2005). In particular, the principal material direction of trabeculae corresponds closely to the

63 principal elastic direction (Odgaard et al., 1997). Barak et al. (2017) recently demonstrated that

64 the principal trabecular orientation represents a robust metric reflecting habitual joint loading

65 differences between chimpanzees and humans in the third metacarpal. When considered together

66 with the phenotypic plasticity of trabecular bone as a site-specific local response (Sugiyama et al.,

67 2012) to locomotor loading (Pontzer et al., 2006; Barak et al., 2011; Wallace et al., 2013), this

68 structure-function relationship provides a direct functional signal of loads incurred during habitual

69 locomotor and postural behavior (Ryan and Ketcham, 2005; Kivell, 2016; Barak et al., 2017).

70 Experimental and comparative work has demonstrated that the principal orientation of trabeculae

71 in a joint reflects the orientation of peak compressive forces experienced during locomotion

72 (Pontzer et al., 2006; Barak et al., 2011, 2013, 2017). Previous work within primates indicates that

73 humans have highly oriented trabeculae (high structural anisotropy) in the femoral head (Ryan and

74 Shaw, 2015), suggesting that trabecular bone organization reflects unique aspects of joint loading

75 during bipedal locomotion (Ryan and Krovitz, 2006; Raichlen et al., 2015), and providing the

76 opportunity to assess whether fossil hominins possess femoral head trabecular bone structure

77 reflective of modern human-like hip joint loading.

78 The goal of this study is to use microcomputed tomography (μCT) to characterize variation in

79 trabecular bone anisotropy, material orientation, and bone volume fraction in the femoral head

80 using a diverse extant primate sample that includes five modern groups of *Homo sapiens*, *Pan*

81 *troglodytes*, *Gorilla* ssp., *Pongo* ssp., and *Papio* ssp. We also assess trabecular bone structure in

82 six specimens of *Australopithecus africanus*, four of *Paranthropus robustus*, and four Pleistocene

83 specimens of *Homo*, including two *Homo neanderthalensis*, one Paleolithic *Homo sapiens*, and

84 the *Homo* sp. femur from Berg Aukas, Namibia. We hypothesize that primate groups that are

85 primarily terrestrial, including quadrupedal baboons and bipedal humans, and therefore exhibit a

86 relatively constrained range of motion at the hip joint, will display more anisotropic hip joint

87 trabecular bone. Further, the primary trabecular bone material orientations in these terrestrial

88 groups will reflect adaptation to repetitive, mostly unidirectional loading. The African apes are

89 primarily terrestrial quadrupeds, but also engage in a variety of locomotor activities on arboreal

90 substrates, including climbing, bridging, and below-branch suspension. As a result, this more

91 diverse loading environment in chimpanzees and gorillas relative to modern humans should be

92 reflected by a relatively more isotropic trabecular bone structure within the hip joint. Orangutans

93 are the most arboreal of the great apes, and therefore should have relatively isotropic femoral head

94 trabecular structure, reflecting their more diverse joint postures and hip joint loading directions. If

95 the trabecular bone degree of anisotropy in the femoral head of australopiths resembles that of

96 modern humans and extinct members of the genus *Homo*, it would indicate that australopiths have

97 rather stereotypical hip joint loading, suggesting less variable hip postures and substrate types. By

98 contrast, if australopith femoral head anisotropy is more like that of extant great apes, it would

99 indicate that, while bipedal, australopiths exhibited much greater variability in hip joint loading

100 conditions and, possibly, more varied substrate use. Bone volume fraction is expected to vary in

101 relation to inferred activity pattern with non-human primates and fossil hominins having higher

102 bone volume compared to Holocene modern humans (Chirchir et al., 2015).

103

104 **2. Materials and methods**

105 *2.1. Sample*

106　　The sample of extant species consisted of adult individuals from five modern populations of

107 *Homo sapiens* ($n = 60$) and four non-human primate taxa (Table 1): *Pan troglodytes* ($n = 17$),

108 *Gorilla* ssp. ($n = 8$; 4 *Gorilla gorilla*, 4 *Gorilla beringei*), *Pongo* ssp. ($n = 7$; 5 *Pongo pygmaeus*,

109 2 *Pongo abelii*), and *Papio* ssp. ($n = 11$; 4 *Papio hamadryas*, 3 *Papio cynocephalus*, 3 *Papio*

110 *ursinus*, 1 *Papio anubis*). See SOM Table S1 for details about extant and fossil specimens used in

111 this study and their museum information. All individuals used in the study were adult based on

112 epiphyseal fusion and free of pathology. Age-at-death estimates for the human samples were taken

113 from museum collection records when available. Most humans in the sample were young adults

114 between 20 and 35 years, although some individuals were as old as 45. The fossil sample included

115 six femora from Sterkfontein assigned to *A. africanus* (StW 99, StW 311, StW 392, StW 403, StW

116   479, StW 501), four femora from Swartkrans attributed to *Paranthropus robustus* (SK 19, SK 82,

117   SK 97, SK 3121), and four Pleistocene *Homo* individuals including the Berg Aukas femur (*Homo*

118   sp.), La Ferrassie 1 and 2 (*Homo neanderthalensis*), and Cro-Magnon 4321 (*Homo sapiens*). We

119   include the StW 311 proximal femur as *A. africanus*, but note that it comes from the younger

120   Sterkfontein Member 5 (Kuman and Clarke, 2000) and therefore may not be attributable to

121   *Australopithecus* (DeSilva, 2011).

122

123   *2.2. Data collection*

124   One proximal femur from each extant individual was scanned using μCT, with voxel

125   dimensions ranging from 0.020 to 0.069 mm. The range of voxel dimensions used from each taxon

126   are listed in Table 1 and voxel sizes for each individual in the sample are listed in the SOM Table

127   S1. Two femora of *Papio hamadryas* were imaged with voxel sizes of 0.069 mm, which were

128   slightly larger than the voxel dimensions used for the other individuals in the sample. Studies have

129   shown that quantification of trabecular bone structure can be affected by scan resolution (Kothari

130   et al., 1998; Sode et al., 2008; Isaksson et al., 2011), although results for these two individuals fall

131   within the range of variation for the other *Papio* individuals analyzed here.

132   We used several μCT scanning facilities, depending on the location of the skeletal and fossil

133   collections (Table 1). In all cases, bones were mounted upright in the scanner and transverse slices

134   were collected with resulting datasets oriented similarly relative to anatomical axes. For specimens

135   scanned on the OMNI-X HD600 μCT scanner at the Penn State Center for Quantitative Imaging

136   (non-human primates, Norris Farms, and Black Earth human groups), voxel dimensions were not

137   isotropic due to the configuration of the scanner. In these scans, the slice thickness was slightly

138   larger than the inline pixel size. The datasets were therefore resampled so that the x,y pixel

139   dimensions matched the slice thickness to create isotropic voxel dimensions. These resampled

140   voxel sizes are the values reported in Table 1 and SOM Table S1. Because a single femur from

141   each individual was scanned from either the left or right side, depending on quality of preservation,

142   all left femora in the sample were mirror imaged, so that they appeared as right side elements. In

143   addition, some scans were inverted in the z-axis. These transformations ensured that all quantified

144   trabecular bone orientation data would be consistent across the sample. In addition, partial

145   australopith femora were oriented using SK 82 as a guide for femoral head positioning. This step

146   was performed in Avizo 9.0 (FEI Visualization Sciences Group, 2017) using 3D isosurfaces to

147   position the femoral head so that the neck shaft angle matched that of SK 82 when oriented in

148   approximate anatomical position.

149   A cubic volume of interest (VOI) was defined in the center of the femoral head bounding box

150   using Avizo 9.0, following previously described methods (Fig. 1; Ryan and Shaw, 2013, 2015).

151   The edge length of each VOI was equal to one-third of the superoinferior height of the articular

152   surface. In the case of StW 99, StW 403, and StW 479, the complete articular surface of the femoral

153   head was not fully preserved. In each of these cases, the bounding box was fit to the maximum

154   extents of the preserved portion of the femoral head and the VOI was extracted from the center of

155   this bounding box. In these three cases, while the VOI was still positioned entirely within the

156   femoral head, it is likely that it was not located in the true center of the femoral head, as in the

157   other specimens. For both SK 82 and La Ferrassie 1, internal damage and cracks were present in

158   the center of the femoral head. Because cracks can have significant effects on quantification of

159   degree of anisotropy (DA) (Bishop et al., 2017), we translated the SK 82 VOI laterally

160   approximately 3.5 mm and the La Ferrassie 1 VOI approximately 3 mm in the lateral, posterior,

161   and superior directions to avoid damaged regions. The translation of these VOIs, although small

162   relative to the overall size of the femoral head, may affect our ability to effectively compare these

163   individuals with others in the sample due to documented effects of VOI position and size on

164   quantification of trabecular bone (Kivell et al., 2011).

165   Each VOI was segmented using an iterative algorithm (Ridler and Calvard, 1978), and the fabric

166   anisotropy and bone volume fraction (BV/TV; bone volume divided by total volume of the VOI)

167   were quantified using the BoneJ plugin (Doube et al., 2010) for ImageJ (Schneider et al., 2012).

168   Due to unique characteristics of preservation for several of the South African fossils, an anisotropic

169   diffusion or 3D median filter was applied prior to segmentation to reduce noise and ensure that the

170   bone/matrix interface was sufficiently distinct for the automatic segmentation. Anisotropy was

171   quantified using the mean intercept length (MIL) method (Odgaard, 1997). The resulting

172   calculated DA values ranged from 0 for an isotropic structure to 1 for a highly anisotropic structure.

173   In addition to the DA, the primary material axes were calculated from the MIL analysis and used

174   to assess variation in the material orientation. Datasets generated for the current study are available

175   from the corresponding author on request.

176
177   *2.3. Statistical analyses*

178   Analysis of variance (ANOVA) was used to assess interspecific differences among the non-

179   human primates, each modern human group, and the australopith species. The cumulative

180   Pleistocene *Homo* sample was not considered in these statistical tests because it is not a natural

181   grouping. Differences in DA and BV/TV between species were assessed with Hochberg's GT2 or

182   Games-Howell post hoc tests, depending on the results of the Levene's test for equality of variance.

183   Cohen's *d* was used to compare effect sizes for between group comparisons of each variable.

184   Pearson correlations were used to address the relationship between BV/TV and DA within each

185   extant species. Statistical analyses were performed in SPSS v24 (IBM Corp., 2016) and R (R

186   Development Core Team, 2013).

187   Primary trabecular orientations were compared with Fisher statistics for directional data in

188   R. Fisher statistics provide a way to assess variation in directional data (Fisher et al., 1987; Butler,

189   1992). All orientations were transformed to be in the positive hemisphere. Orientation data were

190   plotted on equal area stereonet projections. These plots visualize the directional data with each

191   point representing the tip of a vector emanating from the center and terminating on the edge of the

192   sphere. All points are located in the same hemisphere except three *Gorilla* specimens and one *Pan*

193   specimen, which were inverted to facilitate visualization and calculation of Fisher statistics. Fisher

194   statistics for directional data were calculated using the following equations (Fisher et al., 1987;

195   Butler, 1992). The length of the resultant vector (R) was calculated for each species using the

196   equation:

197
$$R^2 = \left(\sum_{i=1}^{N} l_i\right)^2 + \left(\sum_{i=1}^{N} m_i\right)^2 + \left(\sum_{i=1}^{N} n_i\right)^2$$

198   where N is the number of component vectors in the population, and l, m, and n are the direction

199   cosines of the vectors. R approaches N as the orientation of the vectors in the population become

200   more tightly clustered. The precision parameter, k, is an estimate of dispersion and is calculated

201   as:

202
$$k = \frac{N-1}{N-R}$$

203   As R approaches N, the precision parameter k increases. The angular standard deviation (s) is

204   estimated by the following equation:

205
$$s \approx \frac{81°}{\sqrt{k}}$$

206 The 95% confidence limit of the mean, α_{95}, is calculated as an angular radius from the mean with

207 the equation:

208
$$\cos \alpha_{95} = 1 - \frac{N - R}{R}\left\{\left(\frac{1}{0.05}\right)^{1/N-1} - 1\right\}$$

209

3. Results

211   Coronal sections through the proximal femur from a representative individual from each extant

212 taxon and all of the fossils used in the current study are shown in Figure 2. Modern humans and

213 baboons have significantly more anisotropic femoral head trabecular bone (high DA) than

214 chimpanzees, gorillas, and orangutans (Table 2, Fig. 2). ANOVA comparisons indicate significant

215 differences (Table 3) and large effect sizes in DA among the species sampled (Table 4). It is likely

216 that the relatively small standard deviations within human populations contribute to the very large

217 effect sizes observed in DA. Post hoc pairwise comparisons of DA among the five modern human

218 groups revealed only one significant difference. The Norris Farms group has significantly higher

219 DA than the St. John's ($p < 0.01$), but neither group is significantly different than any of the other

220 human groups (Table 4). Although all three ape species tend to overlap the lower range of most of

221 the modern human groups and baboons, all modern human groups and *Papio* have significantly

222 more anisotropic bone than each of the extant ape species (Table 4). The lone exception is the

223 borderline non-significant ($p = 0.056$) pairwise comparison between orangutans and the St. John's

224 group. The three ape species have the highest coefficients of variation, indicating high intraspecific

225 variation in DA, in addition to relatively isotropic, or less organized, trabecular structure. Fossil

226 hominins, including specimens assigned to *Australopithecus africanus* (StW 99, 311, 392, 403,

227 479, 501), *Paranthropus robustus* (SK 19, 82, 97, 3121), and the genus *Homo* (Berg Aukas, La

228 Ferrassie 1, La Ferrassie 2, Cro-Magnon 4321), all have relatively anisotropic femoral head

229 trabecular bone, falling within the cumulative range of variation exhibited by the modern human

230 groups (Fig. 3). The six *A. africanus* specimens appear similar to one another with DA values

231 ranging from 0.54 to 0.68. The femora of *Paranthropus* from Swartkrans have DA values between

232 0.50 and 0.61. The low anisotropy value for SK 82 may have been influenced by the large crack

233 in the femoral head that necessitated slight lateral translation of the VOI. The four Pleistocene

234 *Homo* fossils all have relatively anisotropic trabecular bone, falling within the range of modern

235 humans and baboons, and on the upper end of the range of variation of orangutans. Even though

236 most of the fossils have relatively anisotropic femoral head trabecular bone, we note that fossil

237 specimens SK82, SK97, StW311, StW403, Cro Magnon, and La Ferrassie 1 fall at the upper end

238 or only just outside the ranges of variation for gorillas and chimpanzees. All of the fossils except

239 StW501, StW99, and La Ferrassie 2 overlap the upper end of the range of variation of orangutans.

240   In addition to having significantly more anisotropic trabeculae, primary material orientation in

241 the femoral heads of modern humans is tightly clustered and broadly similar across groups (Fig.

242 4). Mean primary trabecular orientations of individuals within each of the modern human groups

243 were tightly clustered, so they are plotted as one group for the entire species in Fig. 4. The principal

244 material axis in human femoral heads lies medial and slightly anterior to the superoinferior axis

245 (Fig. 4). Modern humans are tightly clustered with high R and k values, the lowest *s* and the

246 smallest α_{95} values of all extant taxa analyzed (Table 2). These tightly clustered material

247 orientation results are also evident within each modern human group, each of which has sample

248 sizes comparable to those of the non-human primates. The main material orientation in baboon

249 femoral heads is similar to those in modern humans, lying slightly medial to the superoinferior

250 axis, but also tends to more frequently lie posterior to the superoinferior axis compared to humans

251 (Fig. 4). Baboons, like human groups, also pair high R and k values together with relatively low s

252 and α_{95}, indicating tightly clustered, uniform main trabecular material orientations. Even though

253 there appears to be general similarity in primary material orientation between baboons and

254 humans, the lack of overlap between the α_{95} confidence ellipses indicates that the mean directions

255 are significantly different between these taxa.

256 In contrast to modern humans and baboons, chimpanzees, gorillas, and orangutans have more

257 dispersed distributions of their primary material axes relative to conspecifics, as each of these taxa

258 exhibit lower values for R and k and larger s and α_{95} confidence limits (Table 2). The higher

259 variation in primary material orientation in apes is likely a correlate of the relatively isotropic, or

260 less organized, trabecular structure in individuals of these taxa. Low DA values indicate somewhat

261 more uniform distribution of bone in all directions within the femoral head. In spite of the

262 significant variation within each species, mean primary fabric directions for chimpanzees and

263 gorillas are similar, lying along a generally posterolateral-anteromedial axis rather than a more

264 superoinferior orientation (Fig. 4). Orangutans have a mean primary fabric direction more closely

265 aligned to that of modern humans and baboons (Fig. 4), but exhibit much larger intragroup

266 variability in primary material orientations, as indicated by the very high α_{95} confidence limit and

267 high dispersion estimate s (Table 2).

268 Primary material axes for nearly all of the individual hominin specimens fall within the range

269 of variation of modern humans. Mean primary material directions for the *Australpithecus* and

270 *Paranthropus* femoral heads lie close to one another with α_{95} confidence ellipses overlapping the

271 mean direction of modern humans and one another, and also falling within the α_{95} confidence limit

272 of orangutans. Fisher statistics indicate relatively tight clustering within both *Australopithecus* and

273 *Paranthropus*, which is more similar to the pattern found in modern human and baboon femoral

274 heads compared with the other hominoids. The four Pleistocene *Homo* specimens all plot within

275 or close to the modern human cumulative range. Both La Ferrassie 1 and 2 are outliers with slightly

276 more posteriorly directed trabeculae that plot just outside of the observed modern human

277 cumulative range of variation.

278   Results for BV/TV indicate a different pattern among the extant and fossil taxa (Fig. 5).

279 ANOVA comparisons indicate significant differences among the species sampled (Table 3). As

280 with the results for DA, effect sizes in comparisons among the human groups and nonhuman

281 primate species are very large and likely attributable to small standard deviations within each

282 human group (Table 5). All modern human groups, except the Black Earth hunter-gatherers, have

283 significantly lower femoral head BV/TV than the extant non-human catarrhine groups (Table 5).

284 The Black Earth group exhibits significantly higher BV/TV compared to all other modern human

285 groups in this analysis, which corroborates their high BV/TV found in earlier analyses (Ryan and

286 Shaw, 2015; Saers et al., 2016). The only other significant pairwise comparison among the modern

287 human groups is the significantly higher BV/TV in the Norris Farms agriculturalists compared to

288 the Inuit. The Norris Farms group overlaps with the lower end of the ranges of non-human

289 catarrhines and the Black Earth group and the upper end of the ranges of the Kerma and St. John's

290 groups. The non-human primate groups generally exhibit a narrower range of intraspecific

291 variation in BV/TV compared to the cumulative modern human sample, based on coefficients of

292 variation for each species as a whole. Among the non-human primate groups, gorillas have the

293 lowest BV/TV values and overlap not only with the Black Earth hunter-gatherers, but also with all

294 of the other human groups except the Inuit.

295 Australopiths have significantly higher BV/TV than all modern human groups, except the Black

296 Earth group (Fig. 5, Table 5). There are no significant differences between *Australopithecus*

297 *africanus* and *Paranthropus robustus*, or between these fossil hominins and the extant non-human

14

298   catarrhine groups in our sample. The four Pleistocene hominin individuals assigned to the genus

299   *Homo* have BV/TV values that fall below the observed range of earlier australopiths, and within

300   the upper half of the observed range of modern human groups, specifically overlapping the Norris

301   Farms early agriculturalist sample. No significant correlations were found between BV/TV and

302   DA in any of the extant groups (Table 6), although the full sample shows a significant but weak

303   correlation (r = -0.33, *n* = 102, *p* < 0.001).

304

305   **4. Discussion**

306   The results of this study demonstrate that *Australopithecus africanus* and *Paranthropus*

307   *robustus* both have highly anisotropic femoral head trabecular bone structure with principal strut

308   orientation similar to that of later hominins and modern humans. If higher trabecular bone

309   anisotropy in the femoral head is indicative of reduced within-individual variability in the

310   directionality of the forces experienced at this joint, as suggested by experimental and modeling

311   data (Christen et al., 2012, 2015), then the increased anisotropy in the femoral heads of

312   *Australopithecus africanus* and *Paranthropus robustus* suggests a narrower range of hip joint

313   postures during locomotion in these taxa than that of African apes. Similarity in principal

314   trabecular bone orientation between australopiths and later hominins suggests similar orientations

315   of peak hip joint compressive loads during locomotion. This indicates that the range of hip joint

316   loading that characterizes habitual bipedalism, and human-like bipedal gait kinematics, had

317   emerged in these hominins. Highly anisotropic bone observed in both hominin bipeds and the

318   predominantly terrestrial quadrupedal baboons suggests that this characteristic is a distinctive

319   functional signal that reflects adaptation to repetitive hip joint reaction forces within a narrow

320   range of hip joint postures during locomotion. Among the diverse modern human groups, femoral

321 head trabecular material is primarily directed slightly medial to the superoinferior axis, which

322 corresponds closely to the observed trajectory of the primary compressive arcade of the proximal

323 femur. This material organization also corresponds to orientations of peak joint reaction forces

324 measured during bipedal walking in living humans outfitted with instrumented hip implants

325 (Bergmann et al., 2001), as well as finite element model-based calculations of peak hip joint forces

326 (Christen et al., 2015). Importantly, variation in fabric anisotropy is independent of the amount of

327 bone present in the hip joint in all taxa analyzed here, suggesting that trabecular anisotropy,

328 specifically, preserves the functional response of bone to joint loading (Pontzer et al., 2006; Polk

329 et al., 2008; Barak et al., 2011).

330 Baboons, like hominins, have a distinct pattern of highly anisotropic trabecular bone structure

331 matching the medial compressive arcade in the femoral head, as noted in previous studies (Fajardo

332 et al., 2007). The primary material orientation of trabeculae in the baboon femoral head is also

333 directed along a trajectory just medial and slightly posterior to the superoinferior axis, as found in

334 some of the human groups. The baboon trabecular trajectory roughly matches the somewhat

335 limited experimental results for hip joint load orientation in quadrupedal dogs and sheep

336 (Bergmann et al., 1984), and hip joint loading data derived from finite element models (Christen

337 et al., 2015). This pattern likely results from the relatively stereotypical loading of the hip joint

338 during pronograde quadrupedal walking, the relative lack of diverse hip joint postures adopted

339 during normal terrestrial locomotion (Rose, 1977), and the more limited range of positional

340 behaviors expressed by baboons compared to chimpanzees (Hunt, 1992), and, presumably, other

341 apes. However, it is important to note, as it is among many modern human populations

342 (Venkataraman et al., 2013), that baboons are not exclusively terrestrial. Many baboon groups

343 regularly use arboreal sleeping sites (Markham et al., 2016), indicating that a stereotypical loading

344 pattern reflected in the architecture of the femoral head does not preclude limited arboreality that

345 may be behaviorally important.

346   In contrast to the pattern of highly anisotropic bone observed in hominins and papionins, the

347 three ape groups have more isotropic femoral head trabecular bone, and importantly, individuals

348 within each of the taxa collectively exhibit more variable primary material orientations relative to

349 one another. All three apes overlap somewhat with the lower range of variation in DA for modern

350 humans and baboons. Orangutans display the highest amount of variation in both DA and principal

351 material orientation, likely reflecting their more varied locomotor postures (Thorpe and Crompton,

352 2006). While the principal fabric direction corresponds to the orientation of peak joint reaction

353 forces during locomotion (Barak et al., 2011, 2013, 2017; Christen et al., 2015), the relatively

354 isotropic trabecular bone of the femoral head in apes strongly suggests that intraindividual hip joint

355 loading in these taxa is sufficiently diverse to maintain a relatively distributed, or isotropic,

356 trabecular structure. This isotropic pattern contrasts with the more uniformly oriented pattern

357 observed in modern humans. The primary material axes in the African apes are positioned along a

358 posterolateral to anteromedial axis, and are therefore quite distinct from all other groups in the

359 study. Although limited, the data on hip joint angles during quadrupedal walking in African apes

360 and orangutans suggest a wider range of hip joint motion within individuals and much higher

361 variability in hip joint angles between individuals compared to bipedal humans (D'Aout et al.,

362 2002; Raichlen et al., 2009; Watson et al., 2009; Pontzer et al., 2014; Finestone et al., 2018) and

363 baboons (Berillon et al., 2010). When walking bipedally, chimpanzees exhibit substantially greater

364 hip abduction and adduction, internal and external rotation of the lower limb, and a less vertical

365 femur than humans (O'Neill et al., 2015). The observed differences in trabecular anisotropy

366 between the predominantly quadrupedal apes (chimpanzees and gorillas) and the quadrupedal

367 baboons may derive from these differences in hip joint kinematics during terrestrial locomotion.

368 A comparatively more diverse range of loading orientations and magnitudes among chimpanzees

369 and gorillas, at least within terrestrial quadrupedalism, may be due to: higher standard deviation

370 in hip joint angles during walking in chimpanzees (Pontzer et al., 2014) compared to baboons

371 (Berillon et al., 2010); and differences in trunk angles between the pronograde baboon and

372 orthograde chimpanzees (Pontzer et al., 2014). To the extent that this difference may not be driven

373 by terrestrial quadrupedalism, it is worth noting that apes perform a broad range of arboreal

374 positional behaviors (Hunt, 1992; Doran, 1997; Carlson, 2005; Thorpe and Crompton, 2006),

375 which also would seem to elicit more diverse hip joint angles. It has also been reported that

376 orangutans adopt highly extended hind limbs during assisted bipedal walking in trees (Thorpe et

377 al., 2007), which may contribute to the more diverse loading and isotropic trabeculae in this taxon.

378 The observed differences in femoral head trabecular bone between quadrupedal baboons and

379 African apes may also derive from phylogenetic differences or differences in the process of

380 endochondral ossification during ontogeny. While the effects of behavioral differences during

381 ontogeny are likely to have a significant impact on femoral head trabecular bone structure (Ryan

382 and Krovitz, 2006; Raichlen et al., 2015), little is known about the role of interspecific differences

383 in ontogenetic processes or phylogeny in determining adult trabecular bone structure.

384   The fourteen fossil hominins included in this analysis span at least five species and yet all have

385 fabric anisotropy characteristics most similar to modern humans, although there is some overlap

386 with the extant apes. This structural correlate for hip loading suggests that habitual bipedalism

387 characterized each taxon, and that hip kinematics were probably broadly human-like. Each of the

388 two South African fossil species has relatively tightly clustered DA values and closely aligned

389 primary material orientations that are nearly indistinguishable from those of some modern humans.

390   The anisotropy of several of the South African fossil specimens overlaps with the upper end of the

391   range of African apes, and nearly all of the hominin fossils overlap the upper end of the orangutan

392   range for DA. This overlap in femoral head anisotropy between the fossil hominins on the one

393   hand and African apes and orangutans on the other, and in primary trabecular orientation between

394   fossil hominins and only orangutans suggests some variability in proximal femoral loading during

395   locomotion both in extinct hominins and extant apes. These results from the hip joint suggest that

396   some arboreal activities in australopiths cannot be definitively excluded. More data are needed to

397   better understand the nature of variation in Pliocene hominin and extant ape trabecular bone

398   structure at the hip joint.

399   The *Homo* fossils from the Late Pleistocene display relatively more variability, with the Cro-

400   Magnon and La Ferrassie femora plotting on the edge or slightly outside the modern human range

401   for primary trabecular orientation. The intraspecific differences in orientation among Neanderthals

402   may result from a suite of derived characteristics of the pelvis and femur (Weaver, 2009; De

403   Groote, 2011). There is little doubt, however, that these members of the genus *Homo* practiced

404   fully modern human-like terrestrial bipedalism that requires an extended hip and knee (Bramble

405   and Lieberman, 2004).

406   Clear structural similarities between the two australopith species and modern human groups

407   suggest that these Pliocene hominins walked with a relatively extended hip, rather than a flexed

408   hip. Due to lower limb kinematic constraints, one may deduce that australopith knee flexion and

409   ankle dorsiflexion would have had to resemble human joint kinematics as well (Schmitt, 2003).

410   Theoretically, joint kinematics during BHBK walking could result in an individual with either

411   more isotropic femoral head trabeculae (i.e., response to a wider range of joint reaction force

412   orientations), or more anterior or ventral positioning of the principal material axis (i.e., response

413   to habitually more flexed hip posture), or even both. The hip joint may present a challenge when

414   trying to decipher BHBK gait in australopiths, however, due to the additional degrees of freedom

415   of movement at this joint compared to other lower limb joints that configurationally emphasize

416   predominantly sagittal plane movements (e.g., knee flexion/extension and ankle

417   dorsiflexion/plantarflexion). However, based on data from bipedally walking chimpanzees (Foster

418   et al., 2013; O'Neill et al., 2015) and bonobos (D'Aout et al., 2002), it seems likely that BHBK gait

419   in australopiths would result in both different hip joint postures and more variable hip loading

420   during the gait cycle compared to modern humans. The observed skeletal differences between

421   modern humans, with a comparatively more limited range of hip joint postures, and extant apes,

422   who engage in more varied locomotor behaviors and a greater range of hip joint positions, suggests

423   that hip loading experienced by these australopith species resembled modern human-like hip

424   loading with a relatively extended hip and knee during walking gaits. This interpretation accords

425   with reconstructions of locomotor behavior and kinematics in australopiths based on trabecular

426   morphology of the ankle and foot (Barak et al., 2013; Zeininger et al., 2016; Su and Carlson, 2017),

427   other morphological characteristics (Ward et al., 2011; Haile-Selassie et al., 2016), kinematic and

428   energetics studies (Wang et al., 2003; Sockol et al., 2007; Crompton et al., 2012; Foster et al.,

429   2013), and fossil trackways (Raichlen et al., 2008, 2010; Crompton et al., 2012).

430   The results of the present study also have the potential to inform our understanding of the degree

431   to which australopiths frequently or habitually engaged in arboreal locomotion. While there is little

432   question that Pliocene hominin postcranial morphology reflects adaptations for committed

433   terrestrial bipedal locomotion (Ward, 2013), evidence from other parts of the skeleton suggests

434   that these early hominins may have engaged in at least some arboreal locomotor activities (Stern,

435   2000; Green and Alemseged, 2012; Marchi, 2015; Ruff et al., 2016; Zeininger et al., 2016; Su and

436 Carlson, 2017). Recent reinterpretations of the A.L. 288-1 fossils of *Australopithecus afarensis*

437 have suggested the potential for a significant arboreal component in the behavioral repertoire of

438 this species (Kappelman et al., 2016; Ruff et al., 2016). Femoral head trabecular bone structure in

439 *Australopithecus africanus* and *Paranthropus robustus*, specifically, indicates hip joint postures

440 and loading patterns that are inconsistent with an ape-like range of arboreal positional behaviors.

441 It seems likely, therefore, that if these australopiths incorporated any arboreality into their

442 locomotor repertoire, they did so less diversely, more infrequently (Ward, 2013), or with hip joint

443 postures and climbing mechanics similar to those used by modern human climbers (Venkataraman

444 et al., 2013) rather than those employed by extant apes (DeSilva, 2009).

445   Anisotropy of femoral head trabecular bone appears to be independent of variation in bone

446 volume fraction. *Australopithecus africanus* and *Paranthropus robustus* both combine a non-

447 human primate-like pattern of robust femoral head trabecular bone (high BV/TV) with highly

448 anisotropic fabric structure (high DA) indicative of locomotor kinematics and hip joint loading

449 like that of later hominins and modern humans. This mismatch between australopith bone mass

450 and anisotropy bolsters the interpretation of fabric anisotropy patterns as a locomotor functional

451 signal, independent of other mechanical, physiological, or nutritional factors affecting skeletal

452 robusticity. Excluding the Black Earth hunter-gatherers, who appear to have uniformly high

453 trabecular bone volume in the hind limb (Saers et al., 2016), there is an almost step-like reduction

454 in BV/TV through time — from the australopiths, to the four Pleistocene *Homo* specimens, to the

455 more recent Holocene modern humans. This high bone volume fraction in the australopith femoral

456 head suggests higher musculoskeletal loading, as implicated by cortical bone structural variation

457 (Ruff et al., 1999, 2016). Higher muscle forces characterizing chimpanzees, and presumably other

458 apes, may also characterize australopiths, with a reduction of power in the genus *Homo* being

459 driven by selection for fine motor control of muscles for tasks demanding dexterity and precision

460 (Walker, 2009), or metabolic tradeoffs associated with increased brain size (Bozek et al., 2014).

461   There is significant variation in femoral head bone volume fraction across the genus *Homo*. The

462 relatively intermediate bone volume fraction results for the Pleistocene *Homo* fossils analyzed here

463 suggest that significantly more variation exists in trabecular bone phenotype across the genus

464 *Homo* than is currently documented (Chirchir et al., 2015). While the fossil sample used in this

465 analysis is small, which is a limitation, the fact that these fossils fall within the range of a more

466 sedentary modern human group (Norris Farms) underscores the potentially important role of non-

467 mechanical factors in driving bone mass variation in later hominins (Devlin, 2015; Weaver et al.,

468 2016).

469   The current study provides valuable insights into the organization of trabecular bone in the

470 femoral heads of baboons, large-bodied hominoids, and living and extinct hominins, but there are

471 several potential limitations to this analysis. The most significant of these limitations are issues

472 associated with the μCT approach including variation in image resolution, VOI specification, and

473 image segmentation. Due to the distribution and variation in the preservation of the collections

474 used in the analysis, multiple different μCT systems and scanning protocols were used in collecting

475 the raw μCT data. This resulted in some variation in image resolution between scans. In most

476 cases, the voxel dimensions were well within the range typical of analyses of trabecular bone

477 structure, especially considering the size of the taxa analyzed. In the case of two baboon

478 individuals, the voxel sizes were slightly larger (0.069 mm) than those used for other individuals

479 in the analysis. The results for these two baboons fall within the range of variation for other

480 baboons, but it is possible that the larger voxel dimensions potentially affected the results for these

481 two individuals.

482   The use of a single VOI rather than quantifying bone structure across the entire joint is also a

483   potential limitation to the study. We positioned the VOIs within the femoral head based on the

484   maximum extents of the articular surface, ensuring that the volumes were homologous in the extant

485   taxa. Due to the nature of preservation in some of the fossils, the articular surfaces were not always

486   complete, so the precise position of the VOI may not have been homologous with the position in

487   the extant species. In addition, in the case of SK82 and La Ferrassie 1, the VOI was translated

488   several millimeters to avoid internal cracks through the trabecular bone, a phenomenon that may

489   have a significant impact on quantification of anisotropy (Bishop et al., 2017). This translation of

490   the VOIs, although small relative to the overall size of the femoral head, may affect the quantified

491   fabric structure results for these individuals (Kivell et al., 2011), which is potentially reflected in

492   the results of these individuals relative to the rest of the hominin sample. A whole bone approach

493   to analyzing trabecular bone structure across the entire femoral head provides an alternative

494   approach that avoids the limitations of the typical VOI method (Gross et al., 2014; Skinner et al.,

495   2015; Kivell, 2016).

496   A final potential limitation related to the μCT approach concerns the segmentation of the fossil

497   specimens. In most cases, the fossil preservation was such that segmentation was straightforward

498   as in the extant sample. However, in the case of several of the fossil hominins, the image data were

499   first filtered to enhance contrast prior to segmentation. The nature of the preservation of these, and

500   many fossils, presents significant challenges for analyses of bone microstructure.

501   In conclusion, phenotypically plastic traits such as trabecular bone and diaphyseal cortical bone

502   structure hold the potential to provide significant insights into the specific behaviors engaged in

503   by individual hominins, allowing for more nuanced reconstructions of locomotor biomechanics,

504   diversity, and evolution (Ward, 2013; Kivell, 2016; Ruff et al., 2016). Broad similarity in

trabecular bone fabric anisotropy and material organization in the femoral heads of all hominins

in this study (especially compared to African apes) suggests overarching similarities in the hip

kinematics between australopiths and later members of the genus *Homo*, including modern

humans. Our data, when considered together with evidence from trabecular bone structure of the

ankle joint (Barak et al., 2013; Su and Carlson, 2017), locomotor kinematics based on fossil

trackways (Raichlen et al., 2010; Crompton et al., 2012; Raichlen and Gordon, 2017), locomotor

energetics (Wang et al., 2003; Sockol et al., 2007), and morphological features of the lower limb

and foot (Ward et al., 2011), indicate that australopiths were human-like in many aspects of their

bipedalism, such as using a relatively extended hip and knee. Further, our data suggest that if

australopiths climbed, they loaded their hip in a manner unlike extant apes, and probably more

similar to modern human climbers (Venkataraman et al., 2013).

538

539

540 **References**
541

542 Barak, M.M., Lieberman, D.E., Hublin, J.J., 2011. A Wolff in sheep's clothing: Trabecular bone
543   adaptation in response to changes in joint loading orientation. Bone 49, 1141–1151.
544 Barak, M.M., Lieberman, D.E., Raichlen, D., Pontzer, H., Warrener, A.G., Hublin, J.J., 2013.
545   Trabecular evidence for a human-like gait in *Australopithecus africanus*. PLoS One 8,
546   e77687.
547 Barak, M.M., Sherratt, E., Lieberman, D.E., 2017. Using principal trabecular orientation to
548   differentiate joint loading orientation in the 3rd metacarpal heads of humans and
549   chimpanzees. Journal of Human Evolution 113, 173–182.
550 Bergmann, G., Deuretzbacher, G., Heller, M., Graichen, F., Rohlmann, A., Strauss, J., Duda,
551   G.N., 2001. Hip contact forces and gait patterns from routine activities. Journal of
552   Biomechanics 34, 859–871.
553 Bergmann, G., Siraky, J., Rohlmann, A., 1984. A comparison of hip joint forces in sheep, dog,
554   and man. Journal of Biomechanics 17, 907–921.
555 Berillon, G., Daver, G., D'Août, K., Nicolas, G., Villetanet, B.D.L., Multon, F., Digrandi, G.,
556   Dubreuil, G., 2010. Bipedal versus quadrupedal hind limb and foot kinematics in a captive
557   sample of *Papio anubis*: setup and preliminary results. International Journal of Primatology
558   31, 159–180.
559 Bishop, P.J., Clemente, C.J., Hocknull, S.A., Barrett, R.S., Lloyd, D.G., 2017. The effects of
560   cracks on the quantification of the cancellous bone fabric tensor in fossil and
561   archaeological specimens: a simulation study. Journal of Anatomy 230, 461–470.
562 Bozek, K., Wei, Y., Yan, Z., Liu, X., Xiong, J., Sugimoto, M., Tomita, M., Paabo, S., Pieszek,
563   R., Sherwood, C.C., Hof, P.R., Ely, J.J., Steinhauser, D., Willmitzer, L., Bangsbo, J.,
564   Hansson, O., Call, J., Giavalisco, P., Khaitovich, P., 2014. Exceptional evolutionary
565   divergence of human muscle and brain metabolomes parallels human cognitive and
566   physical uniqueness. PLoS Biology 12, e1001871.
567 Bramble, D.M., Lieberman, D.E., 2004. Endurance running and the evolution of *Homo*. Nature
568   432, 345–352.
569 Buikstra, J.E., Milner, G.R., 1991. Isotopic and archaeological interpretations of diet in the
570   Central Mississippi Valley. Journal of Archaeological Science 18, 319–329.
571 Butler, R.F., 1992. Paleomagnetism: Magnetic Domains to Geologic Terranes. Blackwell
572   Scientific Publications, Oxford.
573 Carlson, K.J., 2005. Investigating the form-function interface in African apes: relationships
574   between principal moments of area and positional behaviors in femoral and humeral
575   diaphyses. American Journal of Physical Anthropology 127, 312–334.
576 Cessford, C., 2015. The St. John's Hospital cemetery and environs, Cambridge: Contextualizing
577   the Medieval urban dead. Archaeological Journal 172, 52–120.
578 Chirchir, H., Kivell, T.L., Ruff, C.B., Hublin, J.J., Carlson, K.J., Zipfel, B., Richmond, B.G.,
579   2015. Recent origin of low trabecular bone density in modern humans. Proceedings of the
580   National Academy of Sciences USA 112, 366–371.
581 Christen, P., van Rietbergen, B., Lambers, F.M., Muller, R., Ito, K., 2012. Bone morphology
582   allows estimation of loading history in a murine model of bone adaptation. Biomechanics
583   and Modeling in Mechanobiology 11, 483–492.

584 Christen, P., Ito, K., Galis, F., van Rietbergen, B., 2015. Determination of hip-joint loading
585   patterns of living and extinct mammals using an inverse Wolff's law approach.
586   Biomechanics and Modeling in Mechanobiology 14, 427–432.
587 Churchill, S.E., Holliday, T.W., Carlson, K.J., Jashashvili, T., Macias, M.E., Mathews, S.,
588   Sparling, T.L., Schmid, P., de Ruiter, D.J., Berger, L.R., 2013. The upper limb of
589   *Australopithecus sediba*. Science 340, 1233477.
590 Crompton, R.H., Vereecke, E.E., Thorpe, S.K.S., 2008. Locomotion and posture from the
591   common hominoid ancestor to fully modern hominins, with special reference to the last
592   common panin/hominin ancestor. Journal of Anatomy 212, 501–543.
593 Crompton, R.H., Pataky, T.C., Savage, R., D'Aout, K., Bennett, M.R., Day, M.H., Bates, K.,
594   Morse, S., Sellers, W.I., 2012. Human-like external function of the foot, and fully upright
595   gait, confirmed in the 3.66 million year old Laetoli hominin footprints by topographic
596   statistics, experimental footprint-formation and computer simulation. Journal of the Royal
597   Society Interface 9, 707–719.
598 D'Aout, K., Aerts, P., De Clercq, D., De Meester, K., Van Elsacker, L., 2002. Segment and joint
599   angles of hind limb during bipedal and quadrupedal walking of the bonobo (*Pan paniscus*).
600   American Journal of Physical Anthropology 119, 37–51.
601 De Groote, I., 2011. Femoral curvature in Neanderthals and modern humans: a 3D geometric
602   morphometric analysis. Journal of Human Evolution 60, 540–548.
603 DeSilva, J.M., 2009. Functional morphology of the ankle and the likelihood of climbing in early
604   hominins. Proceedings of the National Academy of Sciences USA 106, 6567–6572.
605 DeSilva, J.M., 2011. A shift toward birthing relatively large infants early in human evolution.
606   Proceedings of the National Academy of Sciences USA 108, 1022–1027.
607 DeSilva, J.M., Holt, K., Churchill, S., Carlson, K., Walker, C., Zipfel, B., Berger, L., 2013. The
608   lower limb and mechanics of walking in *Australopithecus sediba*. Science 340, 1232999.
609 Devlin, M.J., 2015. The "Skinny" on brown fat, obesity, and bone. Yearbook of Physical
610   Anthropology 59, 98–115.
611 Doran, D.M., 1997. Ontogeny of locomotion in mountain gorillas and chimpanzees. Journal of
612   Human Evolution 32, 323–344.
613 Doube, M., Kłosowski, M.M., Arganda-Carreras, I., Cordelières, F.P., Dougherty, R.P., Jackson,
614   J.S., Schmid, B., Hutchinson, J.R., Shefelbine, S.J., 2010. BoneJ: Free and extensible bone
615   image analysis in ImageJ. Bone 47, 1076–1079.
616 Dowdeswell, M.R., Jashashvili, T., Patel, B.A., Lebrun, R., Susman, R.L., Lordkipanidze, D.,
617   Carlson, K.J., 2017. Adaptation to bipedal gait and fifth metatarsal structural properties in
618   *Australopithecus*, *Paranthropus*, and *Homo*. Comptes Rendus Palevol 16, 585–599.
619 Fajardo, R.J., Muller, R., Ketcham, R.A., Colbert, M., 2007. Nonhuman anthropoid primate
620   femoral neck trabecular architecture and its relationship to locomotor mode. Anatomical
621   Record 290, 422–436.
622 FEI Visualization Sciences Group, 2017. Avizo 9.0. Hillsboro.
623 Finestone, E.M., Brown, M.H., Ross, S.R., Pontzer, H., 2018. Great ape walking kinematics:
624   Implications for hominoid evolution. American Journal of Physical Anthropology
625   doi:10.1002/ajpa.23397.
626 Fisher, N.I., Lewis, T., Embleton, B.J.J., 1987. Statistical Analysis of Spherical Data. Cambridge
627   University Press, Cambridge.
628 Foster, A.D., Raichlen, D.A., Pontzer, H., 2013. Muscle force production during bent-knee, bent-
629   hip walking in humans. Journal of Human Evolution 65, 294–302.

630 Gebo, D.L., 2014. Primate Comparative Anatomy. Johns Hopkins University Press, Baltimore.

631 Green, D.J., Alemseged, Z., 2012. *Australopithecus afarensis* scapular ontogeny, function, and
632   the role of climbing in human evolution. Science 338, 514–517.

633 Gross, T., Kivell, T.L., Skinner, M.M., Nguyen, N.H., Pahr, D.H., 2014. A CT-image-based
634   framework for the holistic analysis of cortical and trabecular bone morphology.
635   Paleaeontologia Electronica 17, 33A.

636 Haile-Selassie, Y., Saylor, B., Deino, A., Levin, N., Alene, M., Latimer, B., 2012. A new
637   hominin foot from Ethiopia shows multiple Pliocene bipedal adaptations. Nature 483, 565–
638   569.

639 Haile-Selassie, Y., Latimer, B., Lovejoy, C.O., Melillo, S.M., Meyer, M.R., 2016. Conclusion:
640   Implications of KSD-VP-1/1 for early hominin paleobiology and insights into the
641   chimpanzee/human last common ancestor, In: Haile-Selassie, Y., Su, D.F. (Eds.), The
642   Postcranial Anatomy of *Australopithecus afarensis*. Springer, Dordrecht, pp. 179–187.

643 Harcourt–Smith, W., 2016. Early hominin diversity and the emergence of the genus *Homo*.
644   Journal of Anthropological Sciences 94, 19–27.

645 Hatala, K.G., Demes, B., Richmond, B.G., 2016. Laetoli footprints reveal bipedal gait
646   biomechanics different from those of modern humans and chimpanzees. Proceedings of the
647   Royal Society B 283, 20160235.

648 Hunt, K.D., 1992. Positional behavior of *Pan troglodytes* in the Mahale Mountains and Gombe
649   Stream National Parks, Tanzania. American Journal of Physical Anthropology 87, 83–105.

650 IBM Corp., 2016. IBM SPSS Statistics for Windows, Version 24.0. IBM Corp., Armonk, NY.

651 Isaksson, H., Toyras, J., Hakulinen, M., Aula, A.S., Tamminen, I., Julkunen, P., Kroger, H.,
652   Jurvelin, J.S., 2011. Structural parameters of normal and osteoporotic human trabecular
653   bone are affected differently by microCT image resolution. Osteoporosis International 22,
654   167–177.

655 Jefferies, R.W., Lynch, B.M., 1983. Dimensions of Middle Archaic cultural adaptation at the
656   Black Earth Site, Saline County, Illinois, In: Phillips, J.L., Brown, J.A. (Eds.), Archaic
657   Hunters and Gatherers in the American Midwest. Academic Press, New York, pp. 299–
658   322.

659 Kappelman, J., Ketcham, R.A., Pearce, S., Todd, L., Akins, W., Colbert, M.W., Feseha, M.,
660   Maisano, J.A., Witzel., A., 2016. Perimortem fractures in Lucy suggest mortality from fall
661   out of tall tree. Nature 537, 503–507.

662 Kibii, J.M., Churchill, S.E., Schmid, P., Carlson, K.J., Reed, N.D., de Ruiter, D.J., Berger, L.R.,
663   2011. A partial pelvis of *Australopithecus sediba*. Science 333, 1407–1411.

664 Kivell, T.L., 2016. A review of trabecular bone functional adaptation: what have we learned
665   from trabecular analyses in extant hominoids and what can we apply to fossils? Journal of
666   Anatomy 228, 569–594.

667 Kivell, T.L., Skinner, M.M., Lazenby, R., Hublin, J.J., 2011. Methodological considerations for
668   analyzing trabecular architecture: an example from the primate hand. Journal of Anatomy
669   218, 209–225.

670 Kothari, M., Keaveny, T.M., Lin, J.C., Newitt, D.C., Genant, H.K., Majumdar, S., 1998. Impact
671   of spatial resolution on the prediction of trabecular architecture parameters. Bone 22, 437–
672   443.

673 Kuman, K., Clarke, R.J., 2000. Stratigraphy, artefact industries and hominid associations for
674   Sterkfontein, member 5. Journal of Human Evolution 38, 827–847.

Lauder, G.V., 1996. The argument from design, In: Rose, M.R., Lauder, G.V. (Eds.), Adaptation. Academic Press, San Diego, pp. 55–92.

Lovejoy, C.O., 2005a. The natural history of human gait and posture. Part 1. Spine and pelvis. Gait & Posture 21, 95–112.

Lovejoy, C.O., 2005b. The natural history of human gait and posture. Part 2. Hip and thigh. Gait & Posture 21, 113–124.

Lovejoy, C.O., 2007. The natural history of human gait and posture. Part 3. The knee. Gait & Posture 25, 325–341.

Lovejoy, C.O., Suwa, G., Spurlock, L., Asfaw, B., White, T., 2009. The pelvis and femur of *Ardipithecus ramidus*: the emergence of upright walking. Science 326, 71e1–71e6.

Lovejoy, C.O., McCollum, M.A., 2010. Spinopelvic pathways to bipedality: why no hominids ever relied on a bent-hip-bent-knee gait. Philosophical Transactions of the Royal Society B 365, 3289–3299.

Marchi, D., 2015. Using the morphology of the hominoid distal fibula to interpret arboreality in Australopithecus afarensis. Journal of Human Evolution 85, 136–148.

Markham, C., Alberts, S.C., Altmann, J., 2016. Haven for the night: sleeping site selection in a wild primate. Behavioral Ecology 27, 29–35.

Mittra, E., Rubin, C., Qin, Y.-X., 2005. Interrelationships of trabecular mechanical and microstructural properties in sheep trabecular bone. Journal of Biomechanics 38, 1229–1237.

Nagano, A., Umberger, B.R., Marzke, M.W., Gerritsen, K.G., 2005. Neuromusculoskeletal computer modeling and simulation of upright, straight-legged, bipedal locomotion of *Australopithecus afarensis* (A.L. 288-1). American Journal of Physical Anthropology 126, 2–13.

O'Neill, M.C., Lee, L.F., Demes, B., Thompson, N.E., Larson, S.G., Stern, J.T., Jr., Umberger, B.R., 2015. Three-dimensional kinematics of the pelvis and hind limbs in chimpanzee (*Pan troglodytes*) and human bipedal walking. Journal of Human Evolution 86, 32–42.

Odgaard, A., 1997. Three-dimensional methods for quantification of cancellous bone architecture. Bone 20, 315–328.

Odgaard, A., Kabel, J., van Rietbergen, B., Dalstra, M., Huiskes, R., 1997. Fabric and elastic principal directions of cancellous bone are closely related. Journal of Biomechanics 30, 487–495.

Pearson, O.M., Lieberman, D.E., 2004. The aging of Wolff's "law": Ontogeny and responses to mechanical loading in cortical bone. Yearbook of Physical Anthropology 47, 63–99.

Polk, J.D., Blumenfeld, J., Ahluwalia, D., 2008. Knee posture predicted from subchondral apparent density in the distal femur: an experimental validation. Anatomical Record 291, 293–302.

Pontzer, H., Lieberman, D.E., Momin, E., Devlin, M.J., Polk, J.D., Hallgrimsson, B., Cooper, D.M.L., 2006. Trabecular bone in the bird knee responds with high sensitivity to changes in load orientation. Journal of Experimental Biology 209, 57–65.

Pontzer, H., Raichlen, D.A., Rodman, P.S., 2014. Bipedal and quadrupedal locomotion in chimpanzees. Journal of Human Evolution 66, 64–82.

R Development Core Team, 2013. R: A language and environment for statistical computing. R Foundation for Statistical Computing, Vienna.

Raichlen, D.A., Gordon, A.D., 2017. Interpretation of footprints from Site S confirms human-like bipedal biomechanics in Laetoli hominins. Journal of Human Evolution 107, 134–138.

Raichlen, D.A., Pontzer, H., Sockol, M.D., 2008. The Laetoli footprints and early hominin locomotor kinematics. Journal of Human Evolution 54, 112–117.

Raichlen, D.A., Pontzer, H., Shapiro, L.J., Socko, M.D., 2009. Understanding hind limb weight support in chimpanzees with implications for the evolution of primate locomotion. American Journal of Physical Anthropology 138, 395–402.

Raichlen, D.A., Gordon, A.D., Harcourt-Smith, W.E., Foster, A.D., Haas, W.R., 2010. Laetoli footprints preserve earliest direct evidence of human-like bipedal biomechanics. PLoS One 5, e9769.

Raichlen, D.A., Gordon, A.D., Foster, A., Webber, J., Sukhdeo, S., Scott, R., Gosman, J., Ryan, T.M., 2015. An ontogenetic framework linking locomotion and trabecular bone architecture with applications for reconstructing hominin life history. Journal of Human Evolution 81, 1–12.

Rein, T.R., Harrison, T., Carlson, K.J., Harvati, K., 2017. Adaptation to suspensory locomotion in *Australopithecus sediba*. Journal of Human Evolution 104, 1–12.

Ridler, T.W., Calvard, S., 1978. Picture thresholding using an iterative selection method. IEEE Transactions on Systems, Man and Cybernetics SMC-8, 630–632.

Rose, M.D., 1977. Positional behaviour of olive baboons (*Papio anubis*) and its relationship to maintenance and social activities. Primates 18, 59–116.

Rowe, N., 1996. A Pictorial Guide to Living Primates. Pogonias Press, East Hampton.

Ruff, C.B., 1995. Biomechanics of the hip and birth in early *Homo*. American Journal of Physical Anthropology 98, 527–574.

Ruff, C.B., 2010. Body size and body shape in early hominins – implications of the Gona pelvis. Journal of Human Evolution 58, 166–178.

Ruff, C.B., McHenry, H.M., Thackeray, J.F., 1999. Cross-sectional morphology of the SK 82 and 97 proximal femora. American Journal of Physical Anthropology 109, 509–521.

Ruff, C.B., Holt, B., Trinkaus, E., 2006. Who's afraid of the big bad Wolff?:"Wolff's law" and bone functional adaptation. American Journal of Physical Anthropology 129, 484–498.

Ruff, C.B., Burgess, M.L., Ketcham, R.A., Kappelman, J., 2016. Limb bone structural proportions and locomotor behavior in AL 288-1. PLoS One 11, e0166095.

Ryan, T.M., Ketcham, R.A., 2005. The angular orientation of trabecular bone in the femoral head and its relationship to hip joint loads in leaping primates. Journal of Morphology 265, 249–263.

Ryan, T.M., Krovitz, G.E., 2006. Trabecular bone ontogeny in the human proximal femur. Journal of Human Evolution 51, 591–602.

Ryan, T.M., Shaw, C.N., 2015. Gracility of the modern *Homo sapiens* skeleton is the result of decreased biomechanical loading. Proceedings of the National Academy of Sciences USA 112, 372–377.

Ryan, T.M., Shaw, C.N., 2013. Trabecular bone microstructure scales allometrically in the primate humerus and femur. Proceedings of the Royal Society B 280, 20130172.

Saers, J.P., Cazorla-Bak, Y., Shaw, C.N., Stock, J.T., Ryan, T.M., 2016. Trabecular bone structural variation throughout the human lower limb. Journal of Human Evolution 97, 97–108.

Schmitt, D., 2003. Insights into the evolution of human bipedalism from experimental studies of humans and other primates. Journal of Experimental Biology 206, 1437–1448.

Schneider, C.A., Rasband, W.S., Eliceiri, K.W., 2012. NIH Image to ImageJ: 25 years of image analysis. Nature Methods 9, 671–675.

767 Sellers, W.I., Cain, G.M., Wang, W.J., Crompton, R.H., 2005. Stride lengths, speed and energy
768   costs in walking of *Australopithecus afarensis*: using evolutionary robotics to predict
769   locomotion of early human ancestors. Journal of the Royal Society Interface 2, 431–441.
770 Skinner, M.M., Stephens, N.B., Tsegai, Z.J., Foote, A.C., Nguyen, N.H., Gross, T., Pahr, D.H.,
771   Hublin, J.J., Kivell, T.L., 2015. Human evolution. Human-like hand use in
772   *Australopithecus africanus*. Science 347, 395–399.
773 Sockol, M.D., Raichlen, D.A., Pontzer, H., 2007. Chimpanzee locomotor energetics and the
774   origin of human bipedalism. Proceedings of the National Academy of Sciences USA 104,
775   12265.
776 Sode, M., Burghardt, A.J., Nissenson, R.A., Majumdar, S., 2008. Resolution dependence of the
777   non-metric trabecular structure indices. Bone 42, 728–736.
778 Starling, A.P., Stock, J.T., 2007. Dental indicators of health and stress in early Egyptian and
779   Nubian agriculturalists: A difficult transition and gradual recovery. American Journal of
780   Physical Anthropology 134, 520–528.
781 Stern, J.T., 2000. Climbing to the top: A personal memoir of *Australopithecus afarensis*.
782   Evolutionary Anthropology 9, 113–133.
783 Su, A., Carlson, K.J., 2017. Comparative analysis of trabecular bone structure and orientation in
784   South African hominin tali. Journal of Human Evolution 106, 1–18.
785 Sugiyama, T., Meakin, L.B., Browne, W.J., Galea, G.L., Price, J.S., Lanyon, L.E., 2012. Bones'
786   adaptive response to mechanical loading is essentially linear between the low strains
787   associated with disuse and the high strains associated with the lamellar/woven bone
788   transition. Journal of Bone and Mineral Research 27, 1784–1793.
789 Thorpe, S.K.S., Crompton, R.H., 2006. Orangutan positional behavior and the nature of arboreal
790   locomotion in Hominoidea. American Journal of Physical Anthropology 131, 384–401.
791 Thorpe, S.K.S., Holder, R.L., Crompton, R.H., 2007. Origin of human bipedalism as an
792   adaptation for locomotion on flexible branches. Science 316, 1328.
793 Venkataraman, V.V., Kraft, T.S., Dominy, N.J., 2013. Tree climbing and human evolution.
794   Proceedings of the National Academy of Sciences USA 110, 1237–1242.
795 Walker, A., 2009. The strength of great apes and the speed of humans. Current Anthropology 50,
796   229–234.
797 Wallace, I.J., Kwaczala, A.T., Judex, S., Demes, B., Carlson, K.J., 2013. Physical activity
798   engendering loads from diverse directions augments the growing skeleton. Journal of
799   Musculoskeletal & Neuronal Interactions 13, 283–288.
800 Wang, W., Crompton, R.H., Li, Y., Gunther, M.M., 2003. Energy transformation during erect
801   and 'bent-hip, bent-knee' walking by humans with implications for the evolution of
802   bipedalism. Journal of Human Evolution 44, 563–579.
803 Wang, W., Crompton, R.H., Carey, T.S., Gunther, M.M., Li, Y., Savage, R., Sellers, W.I., 2004.
804   Comparison of inverse-dynamics musculo-skeletal models of AL 288-1 *Australopithecus*
805   *afarensis* and KNM-WT 15000 *Homo ergaster* to modern humans, with implications for
806   the evolution of bipedalism. Journal of Human Evolution 47, 453–478.
807 Ward, C.V., 2002. Interpreting the posture and locomotion of *Australopithecus afarensis*: Where
808   do we stand? Yearbook of Physical Anthropology 45, 185–215.
809 Ward, C.V., 2013. Postural and locomotor adaptations of *Australopithecus* species., In: Reed,
810   K.E., Fleagle, J.G., Leakey, R.E. (Eds.), The Paleobiology of *Australopithecus*. Springer,
811   Dordrecht, pp. 235–245.

812   Ward, C.V., Kimbel, W.H., Johanson, D.C., 2011. Complete fourth metatarsal and arches in the
813   foot of *Australopithecus afarensis*. Science 331, 750–753.
814   Watson, J., Payne, R., Chamberlain, A., Jones, R., Sellers, W.I., 2009. The kinematics of load
815   carrying in humans and great apes: implications for the evolution of human bipedalism.
816   Folia Primatologica 80, 309–328.
817   Weaver, C.M., Gordon, C.M., Janz, K.F., Kalkwarf, H.J., Lappe, J.M., Lewis, R., O'Karma, M.,
818   Wallace, T.C., Zemel, B.S., 2016. The National Osteoporosis Foundation's position
819   statement on peak bone mass development and lifestyle factors: a systematic review and
820   implementation recommendations. Osteoporosis International 27, 1–106.
821   Weaver, T.D., 2009. Out of Africa: modern human origins special feature: the meaning of
822   Neandertal skeletal morphology. Proceedings of the National Academy of Sciences USA
823   106, 16028–16033.
824   Zeininger, A., Patel, B.A., Zipfel, B., Carlson, K.J., 2016. Trabecular architecture in the StW 352
825   fossil hominin calcaneus. Journal of Human Evolution 97, 145–158.
826   Zipfel, B., DeSilva, J., Kidd, R., Carlson, K., Churchill, S., Berger, L., 2011. The foot and ankle
827   of *Australopithecus sediba*. Science 333, 1417–1420.
828
829

830

Figure legends

832

Figure 1. VOI selection method. The VOI was placed centrally within the femoral head as
denoted in two dimensions by the red box.

835

Figure 2. Coronal sections through the proximal femur of one individual from each extant taxon
and all fossils used in this analysis. Note that the matrix infilling the intertrabecular spaces in SK
19 and SK 3121 is higher density than the surrounding bone creating the appearance of an
inverted dataset.

840

Figure 3. Boxplots comparing femoral head degree of anisotropy (DA) across extant non-human
catarrhines, modern human groups, and fossil hominin taxa. All volumes of interest were
positioned centrally within the femoral head except for SK 82, which was translated laterally to
avoid a crack, and La Ferrassie 1, which was translated approximately 3 mm laterally,
posteriorly, and superiorly to avoid this damaged region. Colored boxes represent the 50%
interquartile range with the black horizontal line representing the median of each species or
group. Whiskers represent the highest and lowest values, excluding outliers represented as open
circles.

849

Figure 4. Stereonet projections showing principal trabecular material orientations in the femoral
head. (A) Within and between species variation in principal material orientation. (B) Detail of
circular region from A showing extent of variation in principal material directions in modern

853   humans and fossil hominins. (C) Group mean directions with α_{95} confidence limits for each

854   taxon. (D) Detail of mean principal direction and α_{95} confidence limits covering the same region

855   of the graph as in B. Symbols: brown squares = *Pan troglodytes*; green triangles = *Gorilla* ssp.;

856   solid gray diamonds = *Pongo* ssp.; orange triangles = *Papio* ssp.; yellow circles = Holocene

857   modern *Homo sapiens*; red stars = *Australopithecus africanus*; blue crossed circles =

858   *Paranthropus robustus*; green crossed squares = Pleistocene *Homo*. All points represent the tips

859   of vectors emanating from the center and terminating on the edge of a hemisphere. The center of

860   the plot denoted by a black cross represents the superoinferior orientation. All points are in the

861   same hemisphere, except three *Gorilla* and one *Pan* inverted to calculate Fisher statistics. These

862   four specimens are denoted as white triangles (*Gorilla*) or squares (*Pan*).

863

864   **Figure 5.** Boxplots comparing femoral head bone volume fraction across extant non-human

865   catarrhines, modern human groups, and fossil hominin taxa. All volumes of interest were

866   positioned centrally within the femoral head except for SK 82, which was translated laterally to

867   avoid a crack, and La Ferrassie 1, which was translated approximately 3 mm laterally,

868   posteriorly, and superiorly to avoid this damaged region. Colored boxes represent the 50%

869   interquartile range with the black horizontal line representing the median of each species or

870   group. Whiskers represent the highest and lowest values, excluding outliers represented as open

871   circles.

872

Table 1

Taxonomic sample and scanning details.

Taxon	n (f/m/u)	Behavior/subsistence[a]	Voxel size (mm)	Scan location[b]
Extant taxa				
Homo sapiens				
Black Earth	13 (4/9/0)	Hunter-gatherer, semisedentary	0.055	PSU
Inuit	8 (0/0/8)	Hunter-gatherer, seafaring	0.0378	CBC
Norris Farms	15 (8/7/0)	Horticulture	0.057–0.058	PSU
Kerma	10 (2/7/1)	Preindustrial intensive agriculture	0.0378	CBC
St. Johns	14 (5/9/0)	Preindustrial intensive agriculture	0.0378	CBC
Pan troglodytes	17 (4/12/1)	Knuckle-walking/quadrupedalism, climbing	0.051–0.055	PSU
Gorilla ssp.	8 (3/5/0)	Knuckle-walking/quadrupedalism, climbing	0.045–0.052	PSU
Pongo ssp.	7 (2/5/0)	Quadrumanous climbing	0.061	PSU
Papio ssp.	11 (4/3/4)	Terrestrial quadrupedalism	0.037–0.069	PSU
Fossil taxa				
Australopithecus africanus	6			Wits
StW 99			0.030	
StW 311			0.030	
StW 392			0.030	

StW 403		0.030	
StW 479		0.030	
StW 501		0.030	
Paranthropus robustus	4		Wits
SK 19		0.020	
SK 82		0.020	
SK 97		0.021	
SK 3121		0.020	
Pleistocene *Homo* sp.	3		
Berg Aukas		0.045	Wits
La Ferrassie 1		0.050	MNHN
La Ferrassie 2		0.050	MNHN
Cro-Magnon 4321		0.050	MNHN

Abbreviations: f = female; m = male; u = unknown.

[a] Human subsistence descriptions come from Jefferies and Lynch (1983), Buikstra and Milner (1991), Starling and Stock (2007), Cessford (2015), and also museum records. Locomotor descriptions for nonhuman primates come from Gebo (2014) and Rowe (1996).

[b] CBC = Cambridge BioTomography Centre; MNHN= Muséum National d'Histoire Naturelle AST-RX, Paris; PSU = Penn State Center for Quantitative Imaging; Wits = University of the Witwatersrand Microfocus X-ray Computed Tomography facility.

Table 2

Summary statistics for trabecular bone volume fraction (BV/TV) and degree of anisotropy (DA) for each taxon.

Taxon	*n*	BV/TV	BV/TV SD	BV/TV CV	DA	DA SD	DA CV	R	k	s	α95	Mean Direction x	y	z
Papio	11	0.54	0.06	11.85	0.67	0.08	12.24	10.58	24.09	16.50	9.50	0.40	0.18	0.90
Pongo.	7	0.52	0.04	8.18	0.45	0.15	34.20	4.82	2.75	48.81	44.98	0.19	-0.30	0.93
Gorilla	8	0.50	0.06	11.16	0.45	0.10	21.47	7.45	12.82	22.63	16.08	0.57	-0.82	0.03
Pan troglodytes	17	0.60	0.07	12.38	0.39	0.08	21.20	16.07	17.21	19.52	8.85	-0.30	0.91	0.27
Homo sapiens	60	0.39	0.09	23.87	0.63	0.08	12.91	58.99	58.45	10.59	2.42	0.36	-0.09	0.93
Black Earth	13	0.53	0.05	9.76	0.66	0.07	10.46	12.83	71.19	9.60	4.95	0.44	-0.05	0.89
Norris Farms	15	0.41	0.04	10.13	0.69	0.07	10.74	14.80	68.47	9.79	4.65	0.37	-0.17	0.91
Kerma	10	0.34	0.04	10.54	0.61	0.09	14.53	9.91	104.40	7.93	4.75	0.35	-0.06	0.93
Inuit	8	0.29	0.03	10.54	0.60	0.07	11.83	7.83	41.78	12.53	8.67	0.29	-0.01	0.96
St Johns	14	0.35	0.05	14.18	0.58	0.06	9.87	13.79	63.30	10.18	5.03	0.31	-0.09	0.95
Australopithecus africanus	6	0.59	0.07	12.38	0.61	0.06	9.31	5.95	96.26	8.26	6.86	0.37	-0.17	0.91
StW 99		0.66			0.68									
StW 311		0.51			0.54									
StW 392		0.57			0.60									
StW 403		0.63			0.56									

	n													
StW 479		0.67			0.61									
StW 501		0.50			0.67									
Paranthropus robustus	4	0.52	0.03	6.11	0.58	0.07	11.90	3.99	208.75	5.61	6.37	0.39	0.00	0.92
SK 19		0.52			0.65									
SK 82		0.55			0.50									
SK 97		0.48			0.55									
SK 3121		0.54			0.61									
Pleistocene *Homo* sp.	4													
Berg Aukas (*Homo* sp.)		0.45			0.59									
La Ferrassie 1 (*H. neanderthalensis*)		0.43			0.54									
La Ferrassie 2 (*H. neanderthalensis*)		0.39			0.70									
Cro-Magnon 4321 (*H. sapiens*)		0.44			0.54									

Abbreviations: α95 = 95% confidence limit; CV = coefficient of variation; k = precision parameter; R = resultant vector; s = angular standard deviation; SD = standard deviation.

Table 3

ANOVA results for comparisons of degree of anisotropy (DA) and bone volume fraction (BV/TV) among human groups, extant catarrhines, and fossil taxa.

		Sum of squares	df	Mean square	F	*p*
DA	Between groups	1.233	10	0.123	18.112	<0.001
	Within groups	0.694	102	0.007		
	Total	1.927	112			
BV/TV	Between groups	1.231	10	0.123	42.230	<0.001
	Within groups	0.297	102	0.003		
	Total	1.528	112			

Table 4

Cohen's d effect sizes for comparisons of degree of anisotropy (DA) among human groups, extant catarrhines, and fossil taxa. Negative effect sizes indicate higher mean degree of anisotropy in the species or group listed in each row. ANOVA post hoc (Hochberg GT2) results with p-values less than 0.05 are indicated with bold text[a].

	Black Earth	Inuit	Norris Farms	Kerma	St. Johns	*Pan*	*Gorilla*	*Pongo*	*Papio*	*A. africanus*
Inuit	0.819									
Norris Farms	-0.462	-1.233								
Kerma	0.576	-0.147	0.973							
St. Johns	1.238	0.337	**1.671***	0.460						
Pan	**3.518***	**2.696***	**3.859***	**2.655***	**2.662***					
Gorilla	**2.520***	1.712	**2.857***	**1.703**	**1.693***	-0.766				
Pongo	**1.969***	1.284	**2.294***	**1.358**	1.308	-0.589	0.031			
Papio	-0.180	-0.907	0.253	-0.685	1.324	**-3.449***	**-2.439***	**-1.927***		
A. africanus	0.709	-0.161	1.137	0.019	-0.553	**-2.905***	**-1.886***	**-1.338***	0.803	
P. robustus	1.145	0.310	1.528	0.401	0.013	**-2.382**	-1.383	-0.973	1.165	0.524

Table 5

Cohen's d effect sizes for comparisons of bone volume fraction (BV/TV) among human groups, extant catarrhines, and fossil taxa. Negative effect sizes indicate higher mean bone volume fraction in the species or group listed in each row. ANOVA post hoc (Hochberg GT2) results with p-values less than 0.05 are indicated with bold text[a].

	Black Earth	Inuit	Norris Farms	Kerma	St. Johns	*Pan*	*Gorilla*	*Pongo*	*Papio*	*A. africanus*
Inuit	**5.483***									
Norris Farms	**2.638***	**-3.274***								
Kerma	**4.306***	-1.540	1.873							
St. Johns	**3.678***	-1.420	1.387	-0.240						
Pan	-1.007	**-4.900***	**-3.093***	**-4.167***	**-3.927***					
Gorilla	0.630	**-4.782***	**-1.914***	**-3.585***	**-2.953***	**1.443****				
Pongo	0.233	**-6.487***	**-2.667****	**-4.809***	**-3.695***	1.156	-0.443			
Papio	-0.151	**-4.849***	**-2.526***	**-3.905***	**-3.463***	0.813	-0.696	-0.353		
A. africanus	0.964	**-5.811***	**-3.480***	**-4.867***	**-4.273***	0.125	-1.425	-1.168	-0.715	
P. robustus	0.242	**-7.707***	**-2.784***	**-5.343***	**-3.751***	1.124	-0.439	0.008	0.351	1.126

[a] $* = p < 0.05$; $** p < 0.01$, $*** = p < 0.001$.

Table 6

Results of Pearson correlation analyses of BV/TV and DA.

Taxon	r	p	t	df
Papio	0.38	0.25	1.24	9
Pongo	-0.02	0.96	-0.05	5
Gorilla	0.11	0.80	0.27	6
Pan	0.08	0.77	0.30	15
Homo sapiens	0.23	0.08	1.81	58
All extant	-0.30	0.0005	-3.22	101
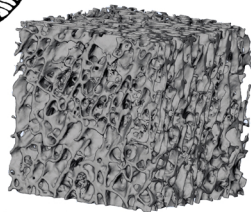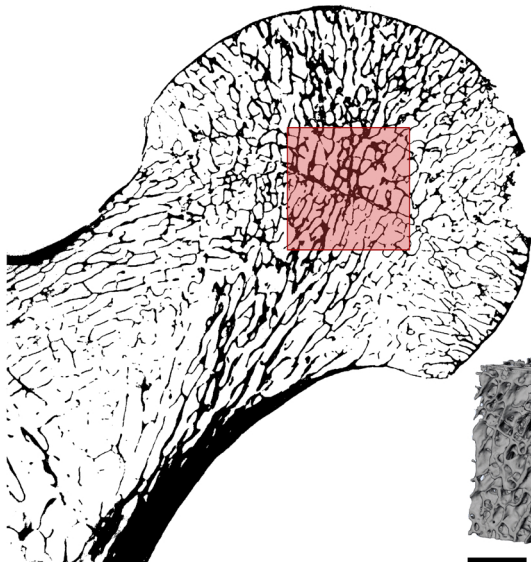
10 mm
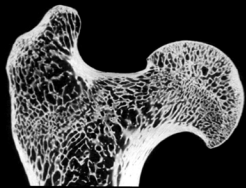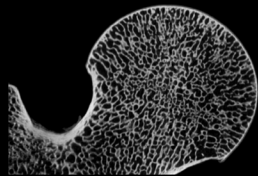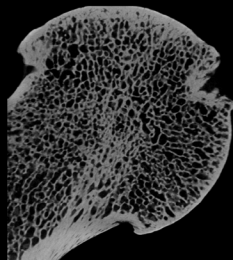
Papio *Pongo* *Gorilla* *Pan* Homo sapiens
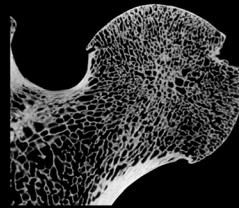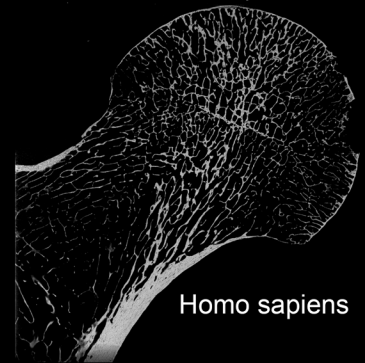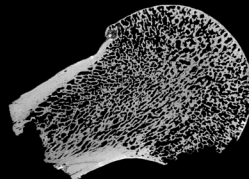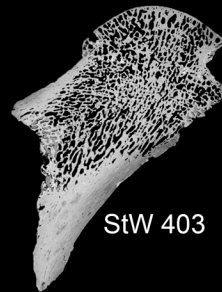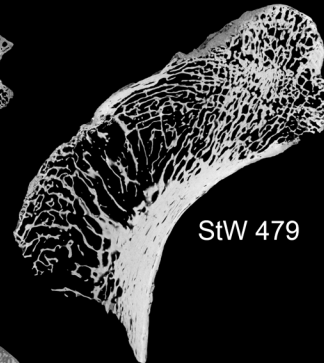
StW 99 StW 311 StW 392 StW 403 StW 479 StW 501
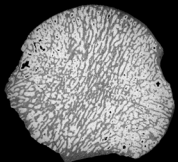
SK 19 SK 82 SK 97 SK 3121

10 mm
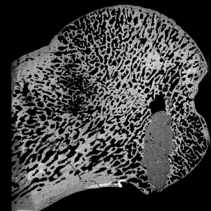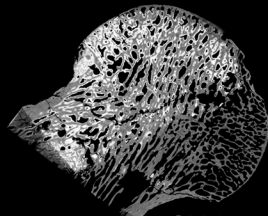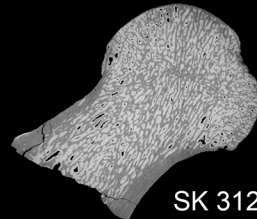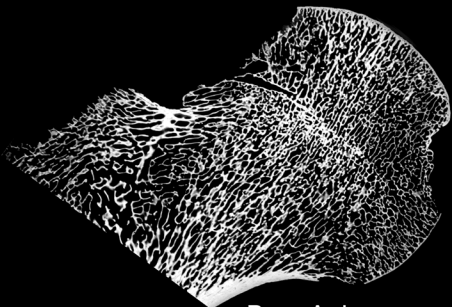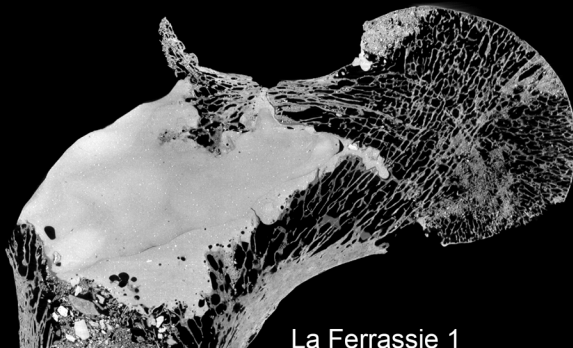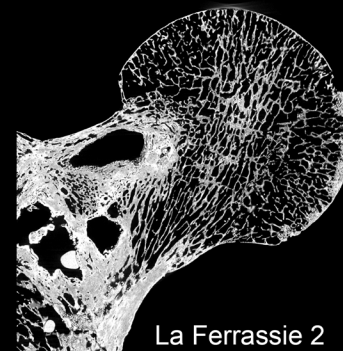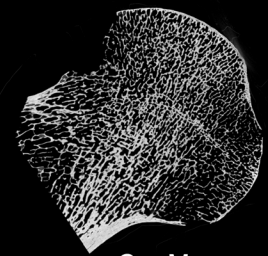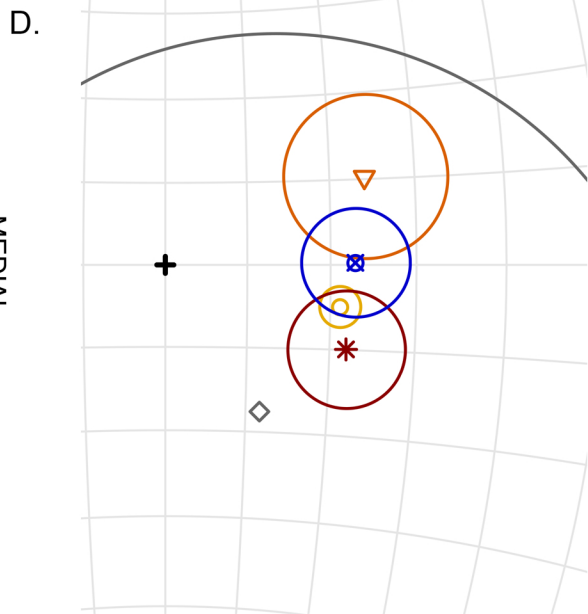
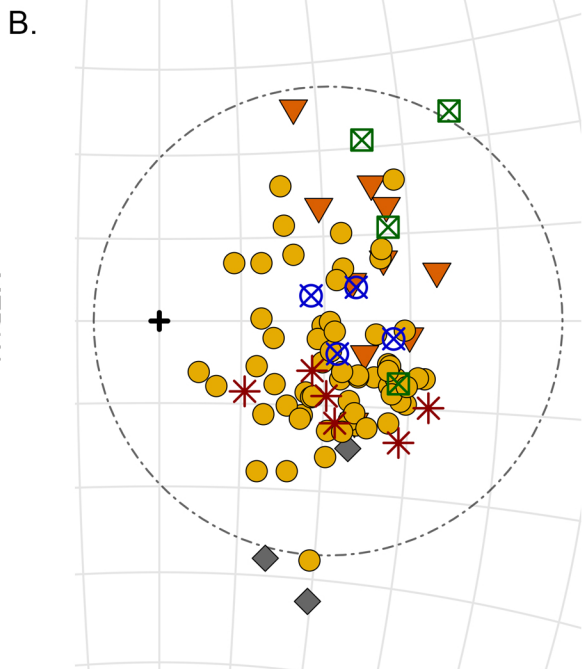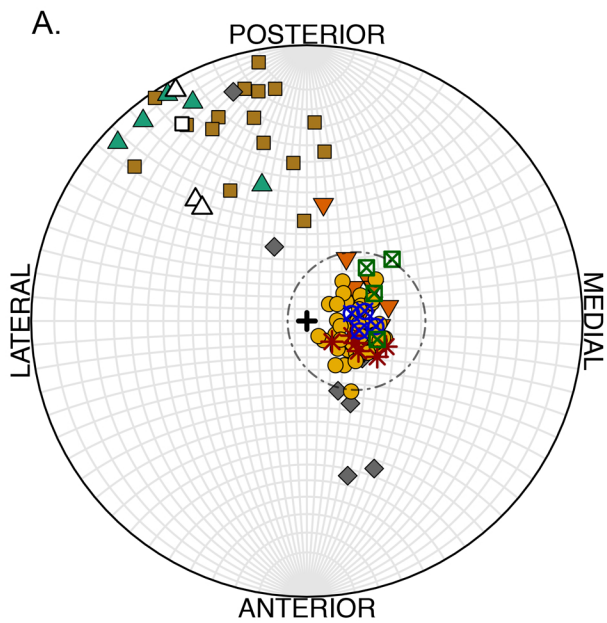Berg Aukas La Ferrassie 1 La Ferrassie 2 Cro Magnon
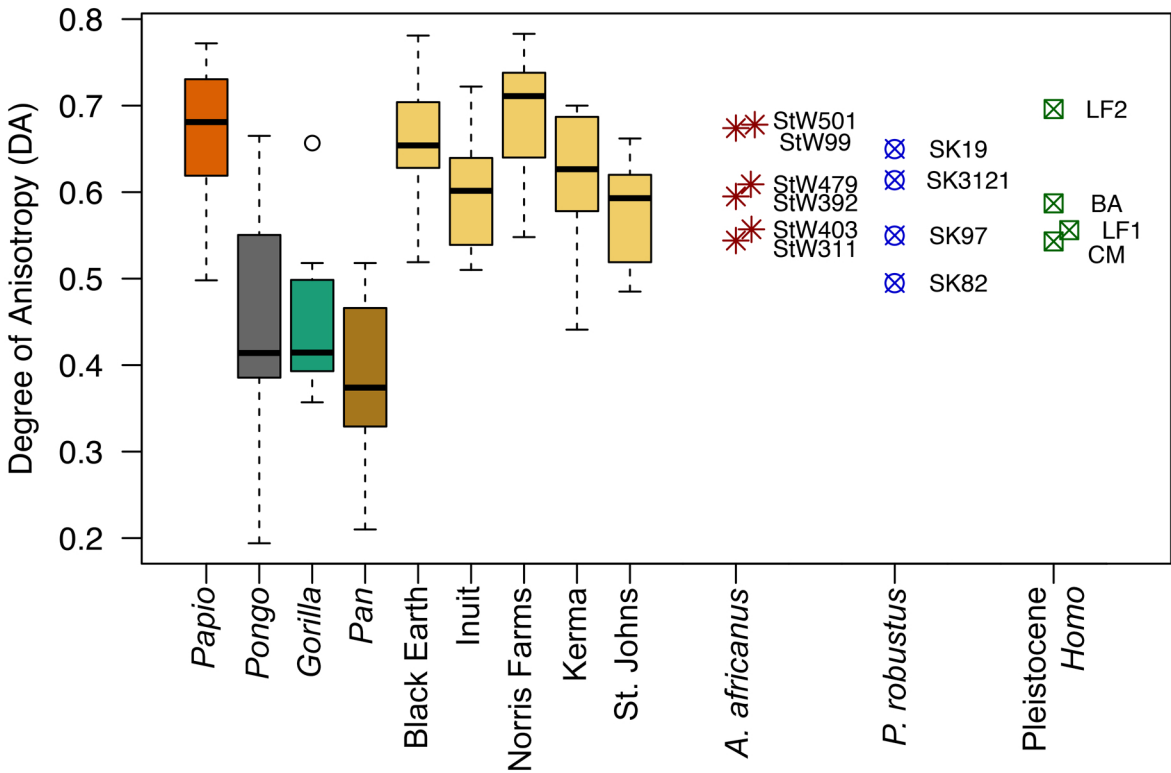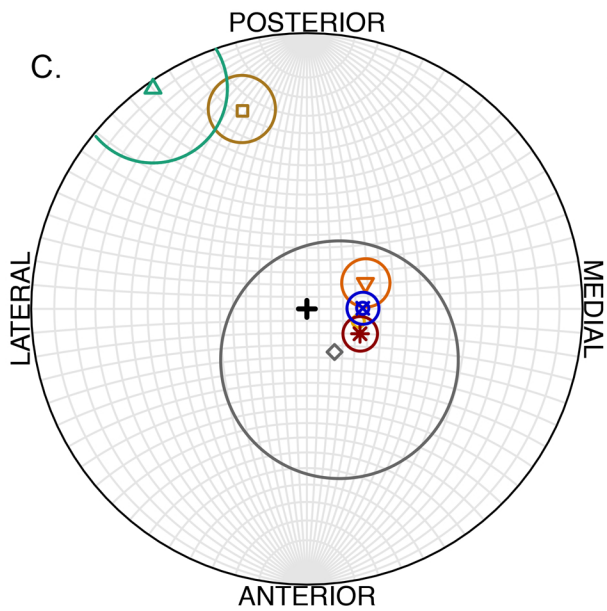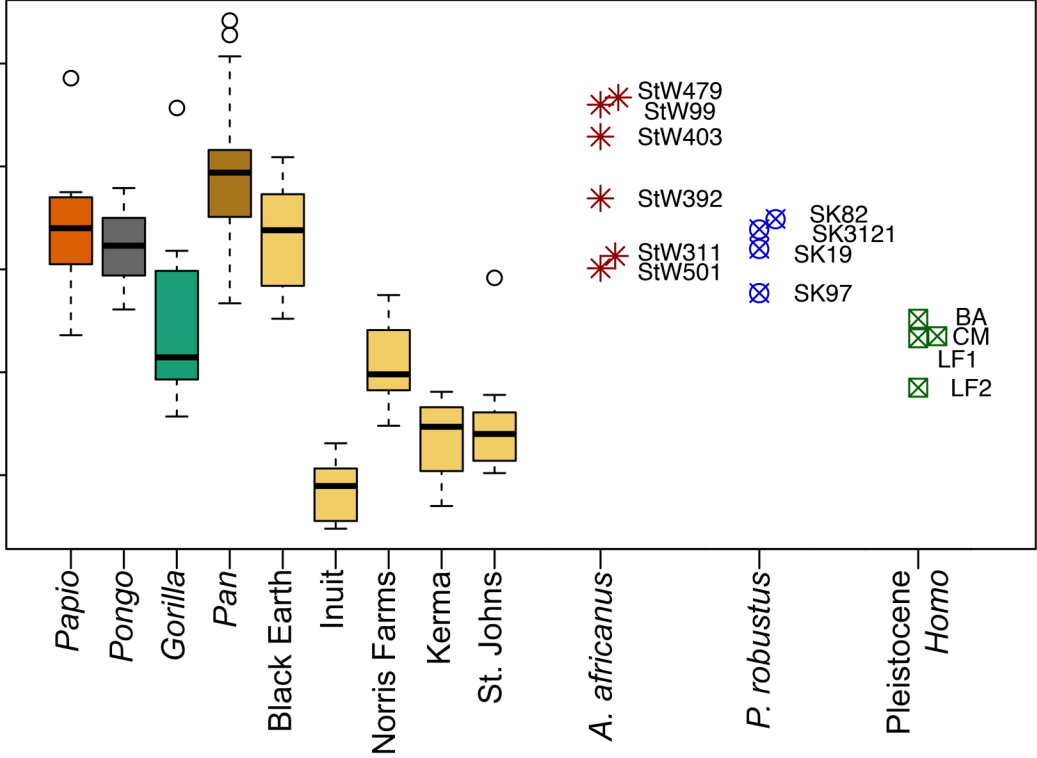
Supplementary Online Material (SOM)

Human-like hip joint loading in *Australopithecus africanus* and *Paranthropus robustus*

Timothy M. Ryan[a,b,*], Kristian J. Carlson[c,d], Adam D. Gordon[e], Nina Jablonski[a], Colin N. Shaw[f], Jay T. Stock[f,g]

[a] *Department of Anthropology, Pennsylvania State University, University Park, PA, USA*

[b] *Center for Quantitative Imaging, Energy and Environmental Sustainability Laboratories,*

Institutes for Energy and the Environment, Pennsylvania State University, University Park, PA,

USA

[c] *Department of Integrative Anatomical Sciences, Keck School of Medicine, University of*

Southern California, Los Angeles, CA, USA

[d] *Evolutionary Studies Institute, University of the Witwatersrand, Johannesburg, South Africa*

[e] *Department of Anthropology, University at Albany - SUNY, Albany, NY, USA*

[f] *PAVE Research Group, Department of Archaeology, University of Cambridge, Cambridge, UK*

[g] *Department of Anthropology, Western University, London, Ontario, Canada, N6A 3K7*

* Corresponding author.

   E-mail address: tmr21@psu.edu (Timothy M. Ryan).

SOM Table S1
Details of skeletal sample.

Species	Group	Museum	Specimen	sex (0=f,1=m,2=u)	Voxel Size
Homo sapiens	Black Earth	Southern Illinois, Carbondale	20B	0	0.055
Homo sapiens	Black Earth	Southern Illinois, Carbondale	22	1	0.055
Homo sapiens	Black Earth	Southern Illinois, Carbondale	33	1	0.055
Homo sapiens	Black Earth	Southern Illinois, Carbondale	50	1	0.055
Homo sapiens	Black Earth	Southern Illinois, Carbondale	86	1	0.055
Homo sapiens	Black Earth	Southern Illinois, Carbondale	99	0	0.055
Homo sapiens	Black Earth	Southern Illinois, Carbondale	106	0	0.055
Homo sapiens	Black Earth	Southern Illinois, Carbondale	110	1	0.055
Homo sapiens	Black Earth	Southern Illinois, Carbondale	113	1	0.055
Homo sapiens	Black Earth	Southern Illinois, Carbondale	141A	1	0.055
Homo sapiens	Black Earth	Southern Illinois, Carbondale	142	1	0.055
Homo sapiens	Black Earth	Southern Illinois, Carbondale	145	0	0.055
Homo sapiens	Black Earth	Southern Illinois, Carbondale	201	1	0.055
Homo sapiens	Norris Farms	Illinois State Museum, Springfield	819941	0	0.058
Homo sapiens	Norris Farms	Illinois State Museum, Springfield	819951	0	0.058
Homo sapiens	Norris Farms	Illinois State Museum, Springfield	819957	0	0.057
Homo sapiens	Norris Farms	Illinois State Museum, Springfield	819963	0	0.058
Homo sapiens	Norris Farms	Illinois State Museum, Springfield	819977	0	0.058
Homo sapiens	Norris Farms	Illinois State Museum, Springfield	819983	1	0.058
Homo sapiens	Norris Farms	Illinois State Museum, Springfield	820647	1	0.058
Homo sapiens	Norris Farms	Illinois State Museum, Springfield	820652	1	0.058
Homo sapiens	Norris Farms	Illinois State Museum, Springfield	820696	1	0.058
Homo sapiens	Norris Farms	Illinois State Museum, Springfield	820715	0	0.058
Homo sapiens	Norris Farms	Illinois State Museum, Springfield	820735	0	0.058
Homo sapiens	Norris Farms	Illinois State Museum, Springfield	820740	1	0.058
Homo sapiens	Norris Farms	Illinois State Museum, Springfield	821042	0	0.058
Homo sapiens	Norris Farms	Illinois State Museum, Springfield	821228	1	0.058
Homo sapiens	Norris Farms	Illinois State Museum, Springfield	821230	1	0.058
Homo sapiens	Kerma	Duckworth Museum, Cambridge	149-745	1	0.038
Homo sapiens	Kerma	Duckworth Museum, Cambridge	610	2	0.038
Homo sapiens	Kerma	Duckworth Museum, Cambridge	704	0	0.038
Homo sapiens	Kerma	Duckworth Museum, Cambridge	737	1	0.038

Homo sapiens	Kerma	Duckworth Museum, Cambridge	759	1	0.038
Homo sapiens	Kerma	Duckworth Museum, Cambridge	781	1	0.038
Homo sapiens	Kerma	Duckworth Museum, Cambridge	783	1	0.038
Homo sapiens	Kerma	Duckworth Museum, Cambridge	849	0	0.038
Homo sapiens	Kerma	Duckworth Museum, Cambridge	1065	1	0.038
Homo sapiens	Kerma	Duckworth Museum, Cambridge	A5	1	0.038
Homo sapiens	Inuit	Duckworth Museum, Cambridge	A'	2	0.038
Homo sapiens	Inuit	Duckworth Museum, Cambridge	Greenland-II	2	0.038
Homo sapiens	Inuit	Duckworth Museum, Cambridge	Greenland_Folio_76	2	0.038
Homo sapiens	Inuit	Duckworth Museum, Cambridge	Labrador_82	2	0.038
Homo sapiens	Inuit	Duckworth Museum, Cambridge	B'	2	0.038
Homo sapiens	Inuit	Duckworth Museum, Cambridge	C'	2	0.038
Homo sapiens	Inuit	Duckworth Museum, Cambridge	E1'	2	0.038
Homo sapiens	Inuit	Duckworth Museum, Cambridge	1929_Folio_80	2	0.038
Homo sapiens	St. Johns	Cambridge Archaeological Unit	2293_3285_394	1	0.038
Homo sapiens	St. Johns	Cambridge Archaeological Unit	2202_2310_805	1	0.038
Homo sapiens	St. Johns	Cambridge Archaeological Unit	2282_3195_364	1	0.038
Homo sapiens	St. Johns	Cambridge Archaeological Unit	2349_3347_917	0	0.038
Homo sapiens	St. Johns	Cambridge Archaeological Unit	2356_3398_935	1	0.038
Homo sapiens	St. Johns	Cambridge Archaeological Unit	2360_3475_958	1	0.038
Homo sapiens	St. Johns	Cambridge Archaeological Unit	2362_3530_970	1	0.038
Homo sapiens	St. Johns	Cambridge Archaeological Unit	2702_1211_184	1	0.038
Homo sapiens	St. Johns	Cambridge Archaeological Unit	2727_2205_264	0	0.038
Homo sapiens	St. Johns	Cambridge Archaeological Unit	2748_3207_367	0	0.038
Homo sapiens	St. Johns	Cambridge Archaeological Unit	2790_1241_709	0	0.038
Homo sapiens	St. Johns	Cambridge Archaeological Unit	2817_1400_768	1	0.038
Homo sapiens	St. Johns	Cambridge Archaeological Unit	2818_1402_769	0	0.038
Homo sapiens	St. Johns	Cambridge Archaeological Unit	2833_2311_809	1	0.038
Pan troglodytes schweinfurthii		American Museum of Natural History	51202	1	0.051
Pan troglodytes schweinfurthii		American Museum of Natural History	51205	2	0.055
Pan troglodytes schweinfurthii		American Museum of Natural History	51376	0	0.055
Pan troglodytes schweinfurthii		American Museum of Natural History	51377	1	0.055
Pan troglodytes schweinfurthii		American Museum of Natural History	51379	1	0.051
Pan troglodytes schweinfurthii		American Museum of Natural History	51381	1	0.055
Pan troglodytes schweinfurthii		American Museum of Natural History	51393	1	0.051
Pan troglodytes verus		American Museum of Natural History	89351	0	0.052

Species	Museum	Catalog	Count	Value
Pan troglodytes verus	American Museum of Natural History	89353	1	0.052
Pan troglodytes verus	American Museum of Natural History	89354	0	0.052
Pan troglodytes verus	American Museum of Natural History	89355	1	0.052
Pan troglodytes verus	American Museum of Natural History	89406	1	0.052
Pan troglodytes verus	American Museum of Natural History	89407	1	0.052
Pan troglodytes troglodytes	American Museum of Natural History	167341	1	0.052
Pan troglodytes troglodytes	American Museum of Natural History	167342	1	0.052
Pan troglodytes troglodytes	American Museum of Natural History	201469	0	0.051
Pan troglodytes	American Museum of Natural History	174861	1	0.052
Pongo abelii	Smithsonian Museum of Natural History	49855	1	0.061
Pongo abelii	Smithsonian Museum of Natural History	49859	1	0.061
Pongo pygmaeus	Smithsonian Museum of Natural History	49769	0	0.061
Pongo pygmaeus	Smithsonian Museum of Natural History	49957	0	0.061
Pongo pygmaeus	Smithsonian Museum of Natural History	49962	1	0.061
Pongo pygmaeus	Smithsonian Museum of Natural History	49967	1	0.061
Pongo pygmaeus	Smithsonian Museum of Natural History	153823	1	0.061
Gorilla gorilla	American Museum of Natural History	54089	1	0.051
Gorilla gorilla	American Museum of Natural History	54090	1	0.051
Gorilla gorilla	American Museum of Natural History	54091	0	0.051
Gorilla gorilla	American Museum of Natural History	54092	0	0.052
Gorilla gorilla	American Museum of Natural History	54355	1	0.045
Gorilla gorilla	American Museum of Natural History	90289	1	0.052
Gorilla gorilla	American Museum of Natural History	90290	1	0.051
Gorilla gorilla	American Museum of Natural History	54327	0	0.052
Papio anubis	Smithsonian Museum of Natural History	162899	1	0.045
Papio cynocephalus	Smithsonian Museum of Natural History	384238	0	0.037
Papio cynocephalus	Smithsonian Museum of Natural History	384239	0	0.037
Papio cynocephalus	Smithsonian Museum of Natural History	452508	0	0.037
Papio hamadryas	American Museum of Natural History	52668	0	0.055
Papio hamadryas	American Museum of Natural History	82096	2	0.069
Papio hamadryas	American Museum of Natural History	82097	2	0.055
Papio hamadryas	American Museum of Natural History	120388	1	0.069
Papio ursinus	American Museum of Natural History	80774	1	0.051
Papio ursinus	American Museum of Natural History	216250	2	0.042
Papio ursinus	American Museum of Natural History	216251	2	0.051

Australopithecus africanus	Evolutionary Studies Institute, University of the Witwatersrand	StW501	–	0.030
Australopithecus africanus	Evolutionary Studies Institute, University of the Witwatersrand	StW99	–	0.030
Australopithecus africanus	Evolutionary Studies Institute, University of the Witwatersrand	StW479	–	0.030
Australopithecus africanus	Evolutionary Studies Institute, University of the Witwatersrand	StW403	–	0.030
Australopithecus africanus	Evolutionary Studies Institute, University of the Witwatersrand	StW311	–	0.030
Australopithecus africanus	Evolutionary Studies Institute, University of the Witwatersrand	StW392	–	0.030
Paranthropus robustus	Ditsong National Museum of Natural History	SK19	–	0.020
Paranthropus robustus	Ditsong National Museum of Natural History	SK82	–	0.020
Paranthropus robustus	Ditsong National Museum of Natural History	SK97	–	0.021
Paranthropus robustus	Ditsong National Museum of Natural History	SK3121	–	0.020
Homo sp.	Evolutionary Studies Institute, University of the Witwatersrand	Berg Aukas	–	0.045
Homo neanderthalensis	Muséum national d'Histoire naturelle	La Ferrassie 1	1	0.050
Homo neanderthalensis	Muséum national d'Histoire naturelle	La Ferrassie 2	0	0.050
Homo sapiens	Muséum national d'Histoire naturelle	Cro-Magnon 1	1	0.050